Low-resolution near-infrared spectroscopic signatures of unresolved ultracool companions to M dwarfs

N. J. Cook,[1,2][*] D. J. Pinfield,[2] F. Marocco,[2] B. Burningham,[2,3] H. R. A. Jones,[2]
J. Frith,[2] J. Zhong,[4] A. L. Luo,[5] Z. X. Qi,[4] N. B. Cowan,[6,7,8,9] M. Gromadzki,[10]
R. G. Kurtev,[11,12] Y. X. Guo,[5] Y. F. Wang,[5] Y. H. Song,[5] Z. P. Yi[13] and R. L. Smart[14]

[1]SC-Physics & Astronomy, Petrie Science & Engineering, 4700 Keele Street, Toronto, ON, M3J 1P3, Canada
[2]Centre for Astrophysics Research, School of Physics, Astronomy, and Mathematics, University of Hertfordshire, College Lane, Hatfield AL10 9AB, UK
[3]NASA Ames Research Center, Mail Stop 245-3, Moffett Field, CA 94035, USA
[4]Key Laboratory for Research in Galaxies and Cosmology, SHAO, Chinese Academy of Sciences, 80 Nandan Road, Shanghai 200030, China
[5]Key Laboratory of Optical Astronomy, NAO, Chinese Academy of Sciences, Datun Road 20A, Beijing 100012, China
[6]Department of Earth and Planetary Sciences, McGill University, 3450 rue University, Montréal, QC H3A 0E8, Canada
[7]Department of Physics, McGill University, 3600 rue University, Montréal, QC H3A 2T8, Canada
[8]McGill Space Institute, 3550 University Street, Montreal, QC H3A 2A7, Canada
[9]Institut de recherche sur les exoplanètes, Département de physique, Université de Montréal, Montréal, QC H3C 3J7, Canada
[10]Warsaw University Astronomical Observatory, Al. Ujazdowskie 4, PL-00-478 Warszawa, Poland
[11]Millennium Institute of Astrophysics, Av. Vicua Mackenna 4860, 782-0436 Macul, Santiago, Chile
[12]Istitiuto de Física y Astronomía, Universidad de Valparaíso, ave. Gran Bretaña, 1111, Casilla 5030, Valparaíso, Chile
[13]Shandong University at Weihai, Weihai 264209, China
[14]Istituto Nazionale di Astrofisica – Osservatorio Astrofisico di Torino, Via Osservatorio 20, I-10023 Torino, Italy

ABSTRACT

We develop a method to identify the spectroscopic signature of unresolved L-dwarf ultracool companions, which compares the spectra of candidates and their associated control stars using spectral ratio differences and residual spectra. We present SpeX prism-mode spectra (0.7–2.5 µm) for a pilot sample of 111 mid-M dwarfs, including 28 that were previously identified as candidates for unresolved ultracool companionship and 83 single M dwarfs that were optically colour similar to these candidates (which we use as 'control stars'). We identify four candidates with evidence for near-infrared excess. One of these (WISE J100202.50+074136.3) shows strong evidence for an unresolved L dwarf companion in both its spectral ratio difference and its residual spectra, two most likely have a different source for the near-infrared excess, and the other may be due to spectral noise. We also establish expectations for a null result (i.e. by searching for companionship signatures around the M dwarf control stars), as well as determining the expected outcome for ubiquitous companionship (as a means of comparison with our actual results), using artificially generated unresolved M+L dwarf spectra. The results of these analyses are compared to those for the candidate sample, and reasonable consistency is found. With a full follow-up programme of our candidates sample from Cook et al., we might expect to confirm up to 40 such companions in the future, adding extensively to the known desert population of M3–M5 dwarfs.
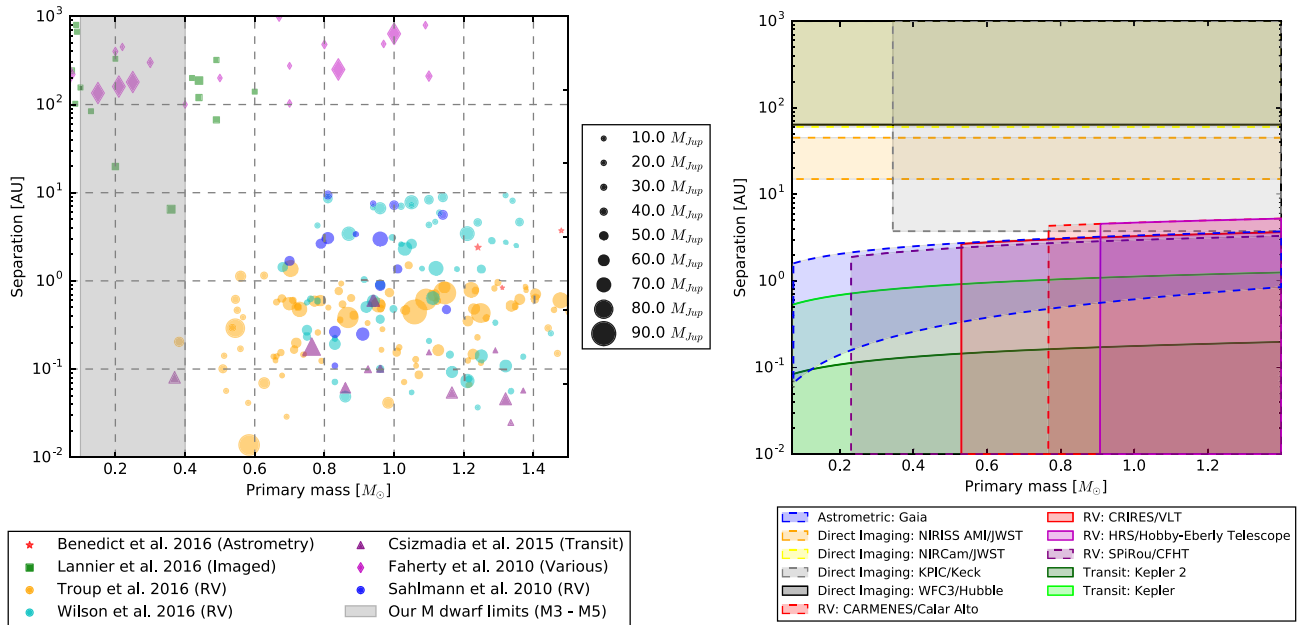
Key words: methods: observational – brown dwarfs – stars: low-mass – infrared: stars.

1 INTRODUCTION

Brown dwarf companions to main-sequence stars are of interest for our understanding of star and brown dwarf formation, as well as for the measurement of brown dwarf properties. The 'brown dwarf desert' was first identified by radial velocity surveys (e.g. Marcy

& Butler 2000), which showed about 5 per cent of solar-type stars have planets ($< 13 M_{\rm Jup}$) within $\sim$5 au, but fewer than 1 per cent of these stars have more massive sub-stellar companions (13–80 $M_{\rm Jup}$) in this separation range. The 'desert' actually extends up to very low mass stellar companions ($\sim$100 $M_{\rm Jup}$), but disappears at higher companion masses for which the frequency is $\sim$10 per cent (Duquennoy & Mayor 1991; Halbwachs et al. 2003). Further study has shown that the desert covers separation ranges out to several hundred au (e.g. Gizis et al. 2001; McCarthy & Zuckerman 2004;

[*] E-mail: neil.james.cook@gmail.com

Figure 1. Left: a representative sample of known UCD companions to low-mass stars, in the separation range <1000 au. Different discovery methods are indicated by different symbols, with symbol size scaling with companion mass (see plot keys). Right: estimated sensitivity regions for different techniques/facilities. We assume the following sensitivity limits: Spatial resolution for *Hubble*/WFC3, *JWST*/NIRISS AMI, *JWST*/NIRCam, Keck/KPIC of 0.4, 0.1–0.3, 0.03, 0.4 arcsec; radial velocity limits for HRS, CRIRES, SPiRou, CARMENES of 3, 5, 4, 1 ms^{-1} (SNR∼100), and baselines for these facilities of 10, 6, 5, 3 yr, respectively; astrometric accuracy for *Gaia* of 150 μas over a 6 yr mission; light-curve accuracy (for transit detection) of 250 and 300 ppm for Kepler and K2 over 3.5 yr and 80 d baselines, respectively.

Cheetham et al. 2015), and also encompasses M dwarfs as well as solar-type stars (Dieterich et al. 2012).

The existence of the desert provides an important test for formation models, with a range of factors potentially contributing to its existence. Jumper & Fisher (2013) suggest turbulent fragmentation alone may give rise to the desert. Alternatively, many brown dwarfs may form in massive circumstellar discs, which only undergo primary fragmentation in their cooler outer parts (Whitworth & Stamatellos 2006; Stamatellos & Whitworth 2009; Li et al. 2015) leading to a desert at closer separation. It has also been suggested close-in brown dwarfs in a protoplanetary disc will undergo inward migration and destruction via a merger with the star (Armitage & Bonnell 2002).

Detailed study of the desert is hampered by the paucity of brown dwarfs, though a desert population has begun to emerge from studies employing radial velocity and astrometry (e.g. Wilson et al. 2016), high-resolution imaging (e.g. Kraus et al. 2011; Dieterich et al. 2012; Hinkley et al. 2015; Mawet et al. 2015), microlensing (e.g. Han et al. 2016) and transit detection (Csizmadia et al. 2015). Indeed, at close separation, the large amount of radial velocity data from exoplanet searches is yielding a more detailed picture (e.g. De Lee et al. 2013; Ma & Ge 2014); however, at wider separations, there are still statistically low numbers of companions.

Desert companions are ultracool dwarfs (UCDs; ≳M8–M9 type and later, ≲2500 K; Chabrier, Gallardo & Baraffe 2007), with their spectral type dependant on mass and age (e.g. see fig. 8 in Burrows et al. 2001). Mid-L dwarfs and cooler objects are all sub-stellar. Early L dwarfs may be low-mass stars older than ∼2 Gyr, high-mass brown dwarfs with an age ∼1–2 Gyr, or younger lower mass brown dwarfs. Late M dwarfs may be low-mass stars (with ages of ∼0.2–1 Gyr or greater) or younger brown dwarfs.

In this paper, we continue our efforts to identify unresolved UCD companions to M dwarfs from the *Sloan Digital Sky Survey* (SDSS;

York et al. 2000), *Two Micron All-Sky Survey* (2MASS; Skrutskie et al. 2006) and *Wide-Field Infrared Survey Explorer* (*WISE*; Wright et al. 2010) compilation of Cook et al. (2016, henceforth Paper I). Our sample is sensitive to projected separations ≲450 au (distances of ∼150 pc at ∼3 arcsec resolution), thus spanning the brown dwarf desert. Fig. 1 shows the observational separation versus primary mass plane for ultracool desert companions. In the left-hand panel, known companions are shown, with different discovery methods and published sources indicated with different symbols, and with symbol size scaled to represent mass. The parameter-space that we explore in this work is shown as a grey region. The right-hand panel shows additional sensitivity regions in this observational plane for a range of other (representative) facilities. These regions are defined through combinations of spatial resolution, radial velocity and astrometric sensitivity, and and observational baseline (see caption for more details). Together these panels show how knowledge of the brown dwarf desert has built up to date, where our new approach contributes and how a range of current/near-future instruments could be capable of measuring new desert discoveries. Our 'search-space' is clearly a relatively unexplored separation range around low-mass M dwarfs, with discoveries having great potential for follow-up study.

We present near-infrared spectroscopic follow-up of a subset of candidate M+UCDs identified by Paper I as M dwarfs with an increased likelihood of ultracool companionship[1]. In Section 2, we summarize the M+UCD candidates, and compare a subset of measured spectral types to our original photometric types. Section 3 describes our spectroscopic method to confirm M+UCD candidates, and presents analysis of synthesized M+UCD systems to gauge

---

[1] Cook et al. (2016) data (the NJCM catalogue) available at http://vizier.cfa.harvard.edu/viz-bin/VizieR?-source=J/MNRAS/457/2192

detection confidence and assess observational requirements. We then describe our initial observations (Section 4) and refinements to our method using this spectroscopy (Section 5). We apply our spectroscopic method to a preliminary set of our M+UCD candidates in Section 6, and discuss the results in Section 7 presenting one strong M+UCD candidate and three additional M dwarfs of interest. Section 8 summarizes our conclusions and discusses potential future work.
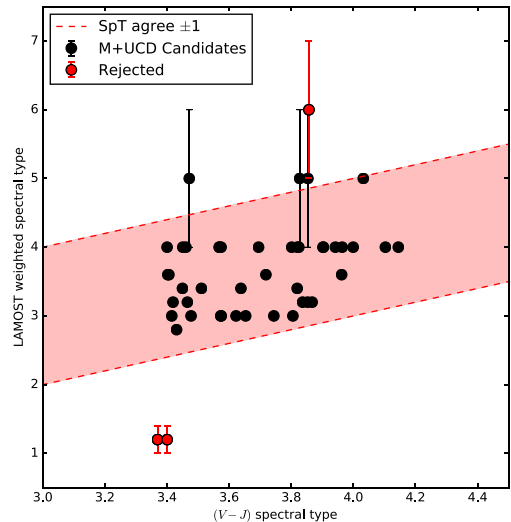
2 A SAMPLE OF CANDIDATE M+UCD SYSTEMS

Our target sample is from the compilation of Paper I. These M dwarf candidates were selected photometrically and cleaned using strict reddening, photometric and quality constraints. Mid-infrared excesses were then assessed in the context of unresolved UCD companionship, by comparing near minus mid-infrared colours (e.g. $J - W2$) amongst subsets of optically colour-similar stars (within 0.01 mag in $g - r$, $g - i$ and $r - i$). A probability analysis then yielded M dwarfs with an increased chance (≥ 4 times that of a random selection) of hosting an unresolved UCD companion. This process identified 1082 M+UCD candidates, and associated colour-similar M dwarfs (to each candidate) in the catalogue. The M+UCD candidates fall into two spectral type bins with 66 per cent M3.5 and 34 per cent M4. The $(J - W2)$ excess for the M3.5 candidates is ~ 0.07 mag (equivalent to $\sim$M8–L3 companions), and for the M4 candidates, it is ~ 0.06 mag (equivalent to $\sim$L0–L4 companions).

Poorly estimated photometric spectral types can lead to spurious M+UCD candidates. For example, underestimated types could lead to an apparent MIR excess in the absence of a UCD companion. In addition, overestimated types could lead to candidates that are too bright intrinsically for measurable UCD excess signatures. To assess how beneficial it would be to have measured spectral types for our full excess sample, we have studied a sub-sample with optical spectral types measured by the *Large sky Area Multi-Object Fibre Spectroscopic Telescope, LAMOST* (Cui et al. 2012; Luo et al. 2012; Zhao et al. 2012). Provided in the LAMOST general catalogues are spectral types determined using a modified version (Luo et al. 2004) of the HAMMER code (Covey et al. 2014). We combined these with spectral types following Zhong et al. (2015), and used a weighted mean where we had multiple spectral types (weighting by $1/\sigma_i^2$, with σ_i the spectral type uncertainty).

To identify M dwarfs that had inconsistent photometric spectral types (such that their M+UCD candidacy must be spurious), we measured the $(V - J)$ range of our candidate selection contours (figs 6 and 7 from Paper I) and converted these into a spectral type range using equation 12 from Lépine et al. (2013). Objects whose true spectral types lie outside of this range are then spurious. Of the 1082 M+UCD candidates, 46 had LAMOST spectra and thus spectral types, of which 3 have photometric spectral types differing significantly from their spectroscopic values (see Fig. 2). We predict only ~ 7 per cent of our candidates have significantly misclassified photometric spectral types. And we thus expect a low level of spurious candidates resulting from photometric mistyping.

As a pilot study, we chose some of the brightest M+UCD candidates from the excess sample of Paper I, as well as a selection of associated colour-similar stars (three per candidate) that we use as control stars in our analysis method. Our selection was prioritized according to (i) the increased probability that a candidate has an unresolved UCD companion, (ii) brightness, (iii) observability and (iv) the availability of bright nearby (on-sky) colour-similar stars. Our observations of these targets will be discussed in Section 4.

Figure 2. Of the 46 M+UCD candidates, three have photometric spectral types that differ significantly from their spectroscopic values. Uncertainties are shown for stars whose spectral types differ significantly from their photometric estimates. We consider a photometrically estimated type to be inconsistent if it differs by ± 1.0 from the spectroscopic value (allowing for measurement uncertainties).

3 SIMULATING UNRESOLVED UCD SPECTROSCOPIC SIGNATURES

In this section, we simulate the near-infrared (NIR) spectroscopic signature of unresolved UCD companions to M3.5–4.5 dwarfs, and establish the basis for our subsequent analysis. Our general approach is to compare the NIR spectrum of an M+UCD candidate to a spectrum of a similar M dwarf that is not expected to have a UCD companion. The comparison M dwarf should have very similar optical and NIR colours to the candidate, and is referred to as a 'control star'. M+UCD candidates were simulated by adding appropriately normalized spectra of an M dwarf and a UCD. Simulated control stars were based on the same M dwarf spectrum (that was used for the M+UCD candidate). However, this spectrum was multiplied through by a normalizing function that was unity at 1.6 and 2.2 μ, but differed by some value at 1.2 μ (we used values giving $\Delta(J-H)$ of ± 0.01, ± 0.02 and ± 0.04 in our analysis). In practice, a cubic spline fit was employed to smoothly interpolate the normalizing function between these fixed values. Our approach relies on a minimum of two control stars (and ideally three) accompanying each candidate in an 'observing group', so that we can compare the results of candidate to control star comparisons with those of control star to control star comparison (where the latter defines the null result).

3.1 Spectral ratio difference

To provide a quantitative statistic for our spectral comparisons, we based our primary comparison on spectral ratios. In the past, spectral ratios have been used to identify unresolved ultracool binaries (e.g. Burgasser et al. 2010) by assessing the spectral morphology of prominent spectral features, and comparing to typical values (for single objects). Since our approach compares candidate spectra to control star spectra (on a case-by-case basis), we instead compare a spectral ratio of a target to that of its control star, i.e. we assess spectral ratio differences (equation 1);

$$\text{Spectral ratio difference} = R_1 - R_2 \tag{1}$$

Table 1. Table of spectral bands used for UCD identification via spectral ratio differences; spectral ratio difference is defined in equation 1. The features these spectral bands relate to can be seen in Fig. 3.[1] From Burgasser et al. (2010).[2] Custom spectral bands based on those of Burgasser et al. (2010) selected to optimize residual spectra while avoiding known telluric features.[3] After experimentation into minimizing the exposure time for observing the band was modified (see Section 3.3).
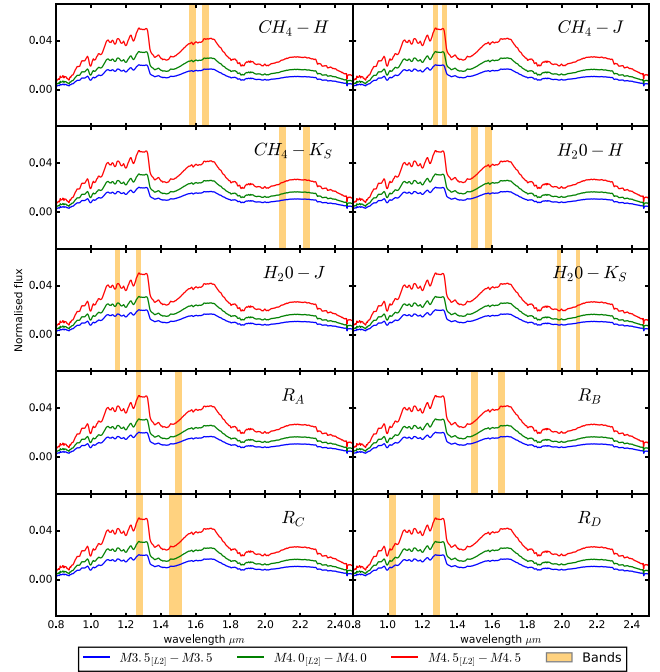
Ratios	Numerator	Denominator	Ref
$H_2O - J$	1.140–1.165	1.260–1.285	1
$CH_4 - J$	1.315–1.340	1.260–1.285	1
$H_2O - H$	1.480–1.520	1.560–1.600	1
$CH_4 - H$	1.635–1.675	1.560–1.600	1
$H_2O - K$	1.975–1.995	2.080–2.100	1
$CH_4 - K$	2.215–2.255	2.080–2.120	1
R_A	1.260–1.285	1.480–1.520	2
R_B	1.635–1.675	1.480–1.520	2
R_C	1.260–1.300	1.450–1.520	2
R_D	1.260–1.300	1.010–1.050	2
R_D^*	1.210–1.350	0.960–1.100	3

where R_1 is the spectral ratio of object 1 and R_2 is the spectral ratio of object 2 (where we use weighted mean flux ratios). This then provides a measure of the difference in spectral morphology between a target spectrum and its control star. We also note if one normalizes both spectra (1 and 2) in the band used as the ratio denominator, the result is a measure of the flux-difference in the numerator (and can be considered as the excess flux normalized in the ratio denominator band). This means that if our numerator targets a maximum in the UCD spectrum and the denominator targets a minimum, our spectral ratio difference will be greatest when a UCD is present in only one of the spectra. To find the optimal ratio, we performed simulations using a variety of bands. The band combinations we assessed were chosen to sample some of the strong NIR absorption features in L dwarf spectra (which are also used in the spectral typing of L dwarfs; Burgasser et al. 2010), while avoiding regions where strong telluric absorption is an issue. In addition to the standard bands, we also included two broadened bands that improve SNR (leading to the R_{D*} ratio). The ratios and bands are shown in Table 1 and Fig. 3 with spectral ratios from Burgasser et al. (2010) shown for comparison.

3.2 Boot-strapped significance

We consider an ideal observing group consisting of an M+UCD candidate plus three control stars, and analyse the spectra using a bootstrap approach. For each wavelength point in the spectra, we generate a Gaussian distribution of 25 flux values (centred on the actual flux value and with a standard deviation equal to the flux uncertainty), thus creating 25 noise-variants for the candidate spectrum and 25 noise-variants for each control star spectrum. We then pair up candidate and control star spectra to yield $(25 + 1)^2 \times 3$ spectral ratio difference values in the presence of an unresolved UCD companion, and pair up control star spectra to yield the same number of spectral ratio difference values in the absence of a UCD companion. These two populations of measurements are then assessed using a t-test to determine the level of significance at which they differ (see equation 2).

$$\text{t-value} = \frac{X - Y}{\sigma_{X-Y}} \qquad \sigma_{X-Y} = \sqrt{\Delta X^2 + \Delta Y^2} \qquad (2)$$

Figure 3. Spectral bands from Table 1. These spectral bands are compared to the subtractions for various M dwarf spectral types. The M3.5 is 2MASS J14113696+2112471 (Kirkpatrick et al. 2010), the M4.5 is 2MASS J12471472-0525130 (Kirkpatrick et al. 2010) and the M5.5 is 2MASS J03023398-1028223 (Burgasser et al. 2004) and the L2 is Kelu-1 (Burgasser 2007).
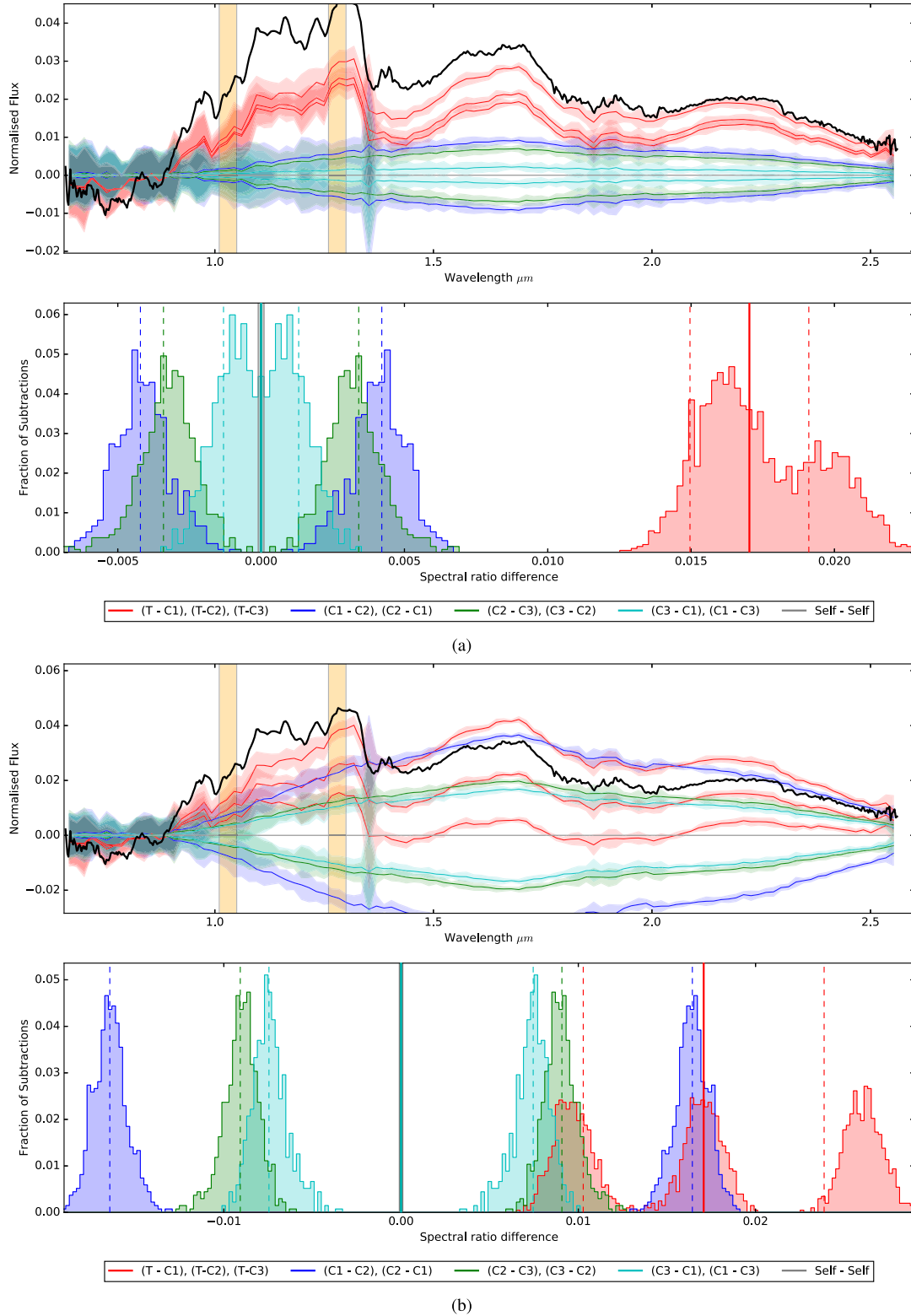
where X is the median of the spectral ratio differences in the presence of a companion, and Y is the median in its absence.

3.3 Optimal ratio bands and observational requirements

We calculated t-values for synthesized M+UCD candidates (according to Sections 3.1 and 3.2) using M3.5, M4.0 and M4.5 types for the primary, and L0, L2, L4 and L6 for the unresolved companion. We find overall, the R_D ratio (1.26–1.3 and 1.01–1.05 µm) leads to the greatest differences for such M+UCD combinations, with the greatest separation between the coloured regions (with a UCD) and the grey regions (where the UCD is absent).

For an M4 dwarf (using the R_D band), a colour similarity of $\Delta(J - H) = \pm0.04$ achieved a t-value of 1.3, for a $\Delta(J - H) = \pm0.02$ the t-value was 2.2 and for $\Delta(J - H) = \pm0.01$ the t-value was 4.6. All control stars were selected to have the lowest $\Delta(J - H)$ possible; in addition to further aid colour-similarity, $\Delta(g - r)$, $\Delta(g - i)$ and $\Delta(r - i)$ were required to be less than 0.01 (as in Paper I). An example of the spectral difference results is shown in Fig. 4 for $\Delta(J - H) = \pm0.01$ and $\Delta(J - H) = \pm0.04$. Through experimentation increasing and decreasing the bandwidth of R_D, we found the best t-values came from extending our bands by ±0.05 µm, corresponding to new spectral bands $R_D^* \equiv$ 1.21–1.35 and 0.96–1.10 µm.

To provide constraints on observational requirements, as well as information about the parameter-space of detectable companions, we investigated expected changes in our t-value results due to differing SNR and resolution ($\delta\lambda/\lambda$; as well as change in primary and secondary spectral type). We ran a series of tests designed to identify the parameters that achieve (i) an optimal result, with t-values in the range 3–5, as well as (ii) a minimal result, with t-values

Figure 4. Residual spectra plot for our simulations (a) $\Delta(J - H) = \pm 0.01$ (b) $\Delta(J - H) = \pm 0.04$. Top panels show the subtractions (target minus control subtractions $= T - CX$ and control minus control subtractions $= CX - CY$, where X and Y refer to the individual control stars). Bottom panels shows the calculated spectral ratio differences for each distribution (equation 1). The M dwarf used here is LP 508-14 (Burgasser et al. 2004) and the UCD is an L2 dwarf, Kelu-1 (Burgasser 2007). Plotted in black is a comparison L0 residual (M4 is LP 508-14, Burgasser et al. 2004, and the L0 is 2MASP J0345432+254023, Burgasser & McElwain 2006).

in the range 2–3, using the shortest possible telescope exposure time (i.e. combination of low SNR and low resolution). We thus require spectroscopy with an SNR of at least 125 and $\delta\lambda/\lambda > 25$. For an optimal result, we require spectroscopy with an SNR $\sim$200 and $\delta\lambda/\lambda \sim 200$. Increasing the SNR can be achieved by reducing the resolution (via binning up the pixels and applying a Gaussian smoothing function).

3.4 Residual spectra

Our spectroscopic difference ratios are indicative of the flux excess in the M+UCD candidates (relative to the control stars, see Section 3.1) when normalized in the denominator band. To obtain a more detailed view of this excess flux, we also plot residual spectra, resulting from both target minus control subtractions and control minus control subtractions. The target minus control subtraction residuals should show a trace of the unresolved UCD spectrum, and the control minus control subtraction residuals should indicate the level of residual excess one can expect for the null case.

Fig. 4 shows the residuals for our simulated spectra (top panels) with target minus control in red, and for control minus control in blue/green/cyan. For comparison, we also plot simulated results for a brighter L0 UCD companion and an ideal case ($\Delta(J - H) = 0$) control star, as a black line.

The bottom panels show histograms of the spectral ratio difference values for the relevant combinations of simulated spectra. The greater the separation between the target minus control distribution and the control minus control distribution, the higher the t-value will be and the more significant the UCD detection. Fig. 5 shows simulation results at reduced SNR (according to Section 3.3).

4 OBSERVATION AND DATA REDUCTION

We obtained low-resolution ($\lambda/\Delta\lambda \sim 150$), near-infrared spectra from SpeX on NASA's *Infrared Telescope Facility* (IRTF; Rayner et al. 2003) using the 0.5×15 arcsec slit (post-upgrade PRISM mode, $\sim$0.7–2.52 μm) on 2016 March 17, 18 and 19 (2016A051, mean seeing of 0.84, 0.85 and 0.70, respectively).

Observations were obtained of 28 M+UCD candidate M dwarfs, and for most of these, we also targeted three colour-similar control stars per candidate (whose optical SDSS colours are within 0.01 mag of the candidate; see Section 2) that were reasonably close in airmass. In one case, we were only able to observe two control stars to accompany the candidate (due to time constraints), leading to a total of 83 control stars being observed (in a standard ABBA fashion). Exposure times[2] were calculated to give an SNR greater than $\sim$150 at 1.05 μm.

We observed each group of M dwarfs (M+UCD candidate plus control stars) consecutively to ensure observing conditions were as similar as possible and also observed one standard star (A0V-type star or similar) close in time and airmass. Flat-fields and argon lamp calibrations were obtained to accompany each group.

The data were reduced using the facility-provided SPEXTOOLS package (Cushing, Vacca & Rayner 2004) that automatically subtracts all AB nods, extracts the spectrum, flat-fields and wavelength calibrates the spectra. We corrected for telluric absorption using the XTELLCOR program (Vacca, Cushing & Rayner 2003). Finally spec-

tra were binned up by a factor of 5 to further increase the SNR. Our spectroscopic observations are summarized in Table 2.

5 IDENTIFYING SPECTRALLY SIMILAR CONTROL STARS

Our pre-observation selection of control stars was based on colour similarity (with associated targets) using available SDSS photometry (see Section 2). With observed spectra in-hand, we also carried out spectroscopic analysis to further improve on this similarity assessment.

We used a reduced chi-squared analysis to compare the optical region of each target with its associated control stars (in the < 1μm range, where a UCD has little-to-no contribution to the flux). As a second condition, we required each target and its associated control stars have similar Y/K flux ratios. We define our Y/K ratio using wavelength bands 1.01–1.05 μm and 2.10–2.30 μm. Within these bands, we expect the flux contribution from a UCD to be relatively low (compared to the wavelength region between these bands).

Control stars were rejected if their spectroscopic difference in the optical (compared to their associated target) amounted to $\chi^2_{\rm Red} > 5$. We also rejected control stars whose Y/K ratio was more than 11.4 per cent different to their associated target, which represents the 2σ range for the full control star sample. Fig. 6 illustrates our rejection procedure for two example groups. In Fig. 6a, no control stars were rejected from the group, and in Fig. 6b, a single control star was rejected as a result of failing both the optical reduced chi-squared condition and the near-infrared Y/K requirement.

Of the 28 observed groups, there were eight groups for which one control star was rejected, and three where two or more control stars were rejected (see Table 3). Groups with two or more rejected control stars were removed from further analysis. Thus, 25 groups with two or three colour and spectroscopically similar control stars were taken forward for further analysis.

6 CANDIDATE AND CONTROL STAR ANALYSIS

For each observation group, we measured spectral ratio differences (see Section 3.1), t-values (see Section 3.2) and spectroscopic residuals (see Section 3.4). Our t-value calculations were made using three different approaches so as to put our final results in a useful context.
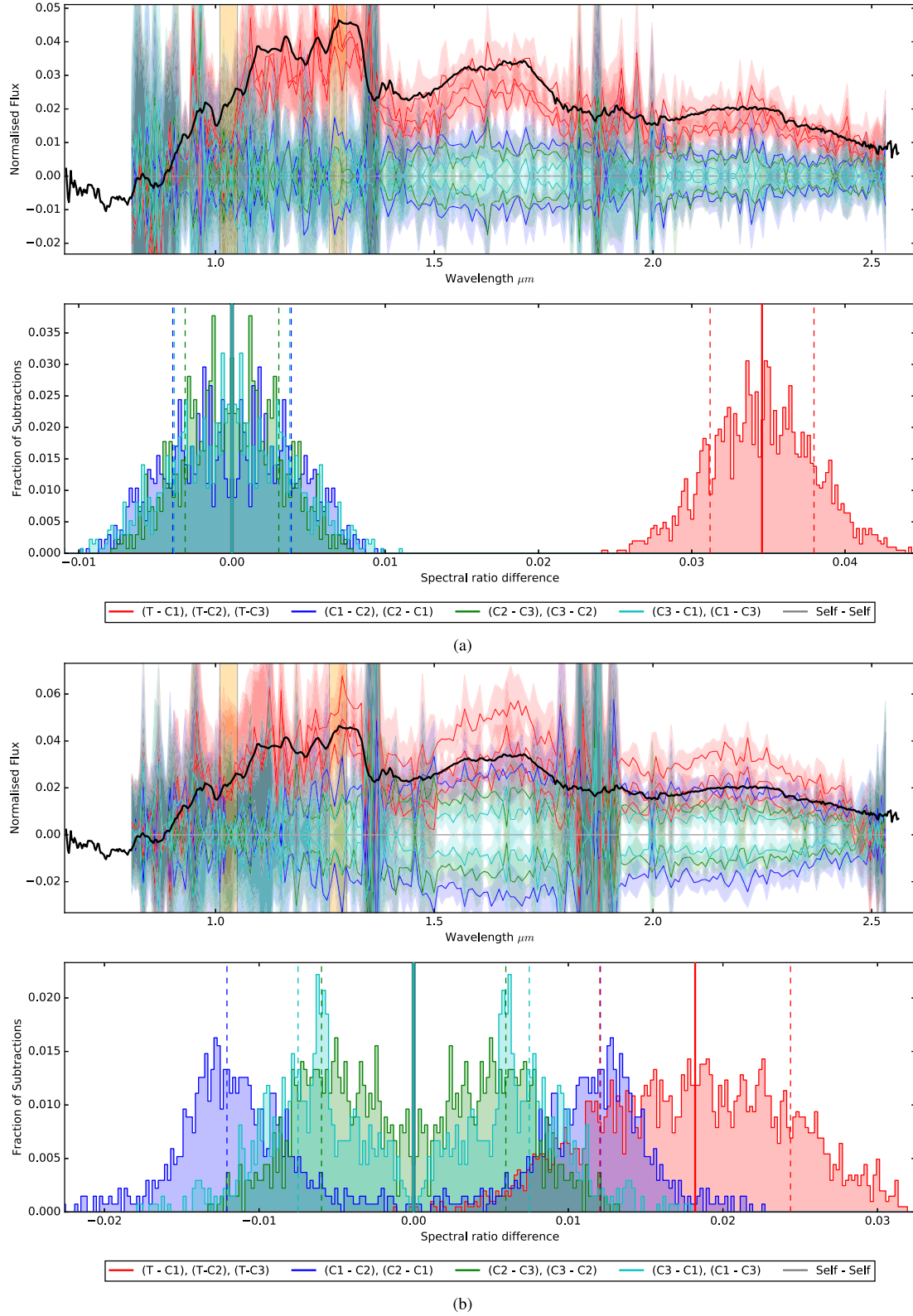
(1) M+UCD candidate minus control
Spectral ratio differences and t-values were calculated for each group using the M+UCD candidate and control star pairings, following the same bootstrap approach described in Section 3.2. This provided a measure for the strength of any unresolved UCD companions around the candidates, and was carried out for the 25 groups with the required number of control stars.

(2) Control star minus control star
For each group, one of the control stars was treated in an identical manner to an M+UCD candidate (in the type 1 analysis), with spectral ratio differences and t-values calculated accordingly. Since the control stars are defined as having no detectable ($J - W2$) excess, any near-infrared excess would presumably come from a non-UCD origin. This therefore allowed us to assess false positives with our data set. We could only carry out this analysis for groups that had three usable control stars, which amounted to 16 of the 25 groups. Thus, we had 48 (16×3) combinations of subtractions (i.e. control

---

[2] Exposure times were calculated using the web-based input form for SpeX http://irtfweb.ifa.hawaii.edu/cgi-bin/spex/spex_calc2.cgi

Figure 5. Residual spectra plot for our simulations where we simulate our observation via lowering the SNR ratio. Layout identical to Fig. 4. (a) A simulated colour-similar M4 subtracted from an M4+L0, SNR = 200, $\delta\lambda/\lambda = 200$, for $\Delta(J-H) = 0.01$ (b) a simulated colour-similar M5 subtracted from an M5+L4, SNR = 200, $\delta\lambda/\lambda = 200$, for $\Delta(J-H) = 0.02$. The M dwarfs are LP 508-14 and Gliese 866AB (M4 and M5, respectively, Burgasser et al. 2004 and Burgasser et al. 2008), the L dwarfs are 2MASP J0345432+254023 and 2MASS J21580457-1550098 (L0 and L4 respectively, Burgasser et al. 2006 and Kirkpatrick et al. 2010). Plotted in black is a comparison L0 residual (M4 is LP 508-14, Burgasser et al. 2004, and the L0 is 2MASP J0345432+254023, Burgasser & McElwain 2006).

Table 2. The groups (target + controls) observed with SpeX in 2016 March. Spectral types, *SpT*, are estimated using $(V - J)$ (see Paper I). α is the right acsension (*WISE*), δ is the declination (WI*a*SE) and *t* is the total exposure time after combining the nods.

WISE ID	Group	Sub-group	α	δ	J [mag]	SpT	Date	t [min]	Airmass
J174613.19+450819.7	7	Target	17:46:13.20	+45:08:19.8	13.26	M3.5	2016/03/17	6.3	1.16
J175142.96+425852.2	7	Control 1	17:51:42.97	+42:58:52.2	13.78	M3.5	2016/03/17	12.5	1.13
J172927.82+431233.5	7	Control 2	17:29:27.82	+43:12:33.5	12.79	M3.5	2016/03/17	3.1	1.10
J154011.95+442100.3	68	Target	15:40:11.95	+44:21:00.3	13.28	M4.0	2016/03/17	6.8	1.10
J154933.69+423709.7	68	Control 1	15:49:33.70	+42:37:09.7	13.43	M4.0	2016/03/17	8.6	1.08
J160029.66+425154.3	68	Control 2	16:00:29.67	+42:51:54.4	12.98	M4.0	2016/03/17	4.1	1.09
J161251.50+462339.6	68	Control 3	16:12:51.51	+46:23:39.7	13.33	M4.0	2016/03/17	7.9	1.12
J151639.28+333630.2	92	Target	15:16:39.29	+33:36:30.2	13.10	M3.5	2016/03/18	5.3	1.04
J150401.20+324758.6	92	Control 1	15:04:01.20	+32:47:58.7	13.84	M3.5	2016/03/18	14.1	1.05
J152114.93+292711.5	92	Control 2	15:21:14.93	+29:27:11.5	13.58	M3.5	2016/03/18	10.8	1.05
J150031.97+382736.6	92	Control 3	15:00:31.97	+38:27:36.7	13.35	M3.5	2016/03/18	8.6	1.15
J150642.41+324609.9	109	Target	15:06:42.41	+32:46:10.0	12.39	M3.5	2016/03/18	2.4	1.03
J150615.82+354711.6	109	Control 1	15:06:15.82	+35:47:11.6	13.07	M3.5	2016/03/18	5.5	1.04
J152258.45+322504.6	109	Control 2	15:22:58.46	+32:25:04.7	12.39	M3.5	2016/03/18	2.4	1.02
J153743.30+324043.3	109	Control 3	15:37:43.31	+32:40:43.4	13.34	M3.5	2016/03/18	7.9	1.02
J144928.03+111712.9	124	Target	14:49:28.04	+11:17:13.0	13.31	M4.0	2016/03/19	6.9	1.05
J145825.27+134738.3	124	Control 1	14:58:25.28	+13:47:38.4	13.05	M4.0	2016/03/19	4.7	1.06
J145830.49+171004.9	124	Control 2	14:58:30.49	+17:10:04.9	13.92	M4.0	2016/03/19	13.9	1.08
J151527.31+061054.6	124	Control 3	15:15:27.31	+06:10:54.6	13.72	M4.0	2016/03/19	12.5	1.13
J143046.74+272058.2	159	Target	14:30:46.74	+27:20:58.2	13.76	M3.5	2016/03/17	12.8	1.01
J143927.22+265329.4	159	Control 1	14:39:27.22	+26:53:29.5	12.93	M3.5	2016/03/17	3.3	1.01
J141757.86+271555.8	159	Control 2	14:17:57.86	+27:15:55.9	13.72	M3.5	2016/03/17	11.9	1.02
J141352.49+264653.7	159	Control 3	14:13:52.49	+26:46:53.8	13.73	M3.5	2016/03/17	11.4	1.03
J140145.91+310640.6	228	Target	14:01:45.91	+31:06:40.6	13.72	M3.5	2016/03/19	12.4	1.03
J141754.96+303827.4	228	Control 1	14:17:54.97	+30:38:27.5	13.52	M3.5	2016/03/19	9.7	1.04
J142140.35+263145.0	228	Control 2	14:21:40.35	+26:31:45.1	12.86	M3.5	2016/03/19	3.7	1.02
J133620.38+275852.6	228	Control 3	13:36:20.39	+27:58:52.7	13.98	M3.5	2016/03/19	17.2	1.14
J135939.98+271349.3	232	Target	13:59:39.98	+27:13:49.4	12.79	M3.5	2016/03/18	2.9	1.01
J135919.47+245242.7	232	Control 1	13:59:19.48	+24:52:42.7	13.49	M3.5	2016/03/18	9.4	1.00
J140311.76+294227.6	232	Control 2	14:03:11.77	+29:42:27.6	13.36	M3.5	2016/03/18	8.3	1.02
J140922.06+320938.0	232	Control 3	14:09:22.06	+32:09:38.1	13.30	M3.5	2016/03/18	7.3	1.03
J133709.98+051838.0	282	Target	13:37:09.99	+05:18:38.0	13.60	M3.5	2016/03/18	9.7	1.05
J135037.01+052648.3	282	Control 1	13:50:37.02	+05:26:48.4	13.69	M3.5	2016/03/18	11.3	1.05
J135218.99+065447.2	282	Control 2	13:52:19.00	+06:54:47.2	12.93	M3.5	2016/03/18	3.3	1.03
J135342.62+030317.3	282	Control 3	13:53:42.62	+03:03:17.3	12.89	M3.5	2016/03/18	3.7	1.02
J131246.68+301857.5	340	Target	13:12:46.68	+30:18:57.6	13.65	M4.0	2016/03/19	11.1	1.02
J133526.02+291402.1	340	Control 1	13:35:26.03	+29:14:02.1	13.85	M4.0	2016/03/19	14.3	1.01
J134722.80+314804.7	340	Control 2	13:47:22.80	+31:48:04.7	13.68	M4.0	2016/03/19	11.4	1.03
J132515.09+224902.4	340	Control 3	13:25:15.09	+22:49:02.4	13.14	M4.0	2016/03/19	5.9	1.04
J130340.78+152551.9	360	Target	13:03:40.78	+15:25:51.9	12.78	M3.5	2016/03/17	2.9	1.00
J132523.20+174000.9	360	Control 1	13:25:23.21	+17:40:01.0	13.62	M3.5	2016/03/17	10.7	1.00
J124919.38+210618.2	360	Control 2	12:49:19.39	+21:06:18.3	12.85	M3.5	2016/03/17	3.3	1.03
J131145.84+084345.0	360	Control 3	13:11:45.84	+08:43:45.1	13.66	M3.5	2016/03/17	11.4	1.04
J122352.96+052659.9	466	Target	12:23:52.97	+05:26:59.9	12.96	M3.5	2016/03/17	3.8	1.04
J122932.96+075423.5	466	Control 1	12:29:32.96	+07:54:23.6	13.14	M3.5	2016/03/17	5.3	1.02
J120916.25+051754.2	466	Control 2	12:09:16.25	+05:17:54.3	13.67	M3.5	2016/03/17	10.1	1.02
J125055.41+043050.3	466	Control 3	12:50:55.41	+04:30:50.3	13.96	M3.5	2016/03/17	16.5	1.04
J122043.33+203120.6	476	Target	12:20:43.34	+20:31:20.7	13.32	M4.0	2016/03/19	7.1	1.00
J124740.40+233615.7	476	Control 1	12:47:40.41	+23:36:15.7	12.73	M3.5	2016/03/19	3.1	1.00
J121822.55+285654.2	476	Control 2	12:18:22.55	+28:56:54.3	12.79	M3.5	2016/03/19	3.1	1.02
J114605.14+234707.5	476	Control 3	11:46:05.15	+23:47:07.6	14.01	M4.0	2016/03/19	16.9	1.05
J114857.72+073046.3	550	Target	11:48:57.73	+07:30:46.3	12.68	M4.0	2016/03/18	2.7	1.02
J122213.43+091128.9	550	Control 1	12:22:13.44	+09:11:29.0	13.64	M4.0	2016/03/18	9.9	1.02
J122200.86+121753.1	550	Control 2	12:22:00.86	+12:17:53.1	13.13	M4.0	2016/03/18	5.7	1.01
J115522.06+002657.3	550	Control 3	11:55:22.07	+00:26:57.3	12.03	M4.0	2016/03/18	2.1	1.09
J104507.41+181311.0	697	Target	10:45:07.41	+18:13:11.1	12.36	M3.5	2016/03/18	2.3	1.01
J104540.21+174228.0	697	Control 1	10:45:40.22	+17:42:28.0	12.46	M3.5	2016/03/18	2.5	1.01
J110355.23+153411.7	697	Control 2	11:03:55.23	+15:34:11.7	12.00	M3.5	2016/03/18	2.1	1.02
J111056.11+180251.5	697	Control 3	11:10:56.12	+18:02:51.5	13.28	M3.5	2016/03/18	7.5	1.01
J102239.45+053345.5	751	Target	10:22:39.46	+05:33:45.6	13.13	M3.5	2016/03/17	5.7	1.04
J103128.01+054011.4	751	Control 1	10:31:28.01	+05:40:11.4	14.11	M3.0	2016/03/17	18.9	1.04

Table 2 – *continued*

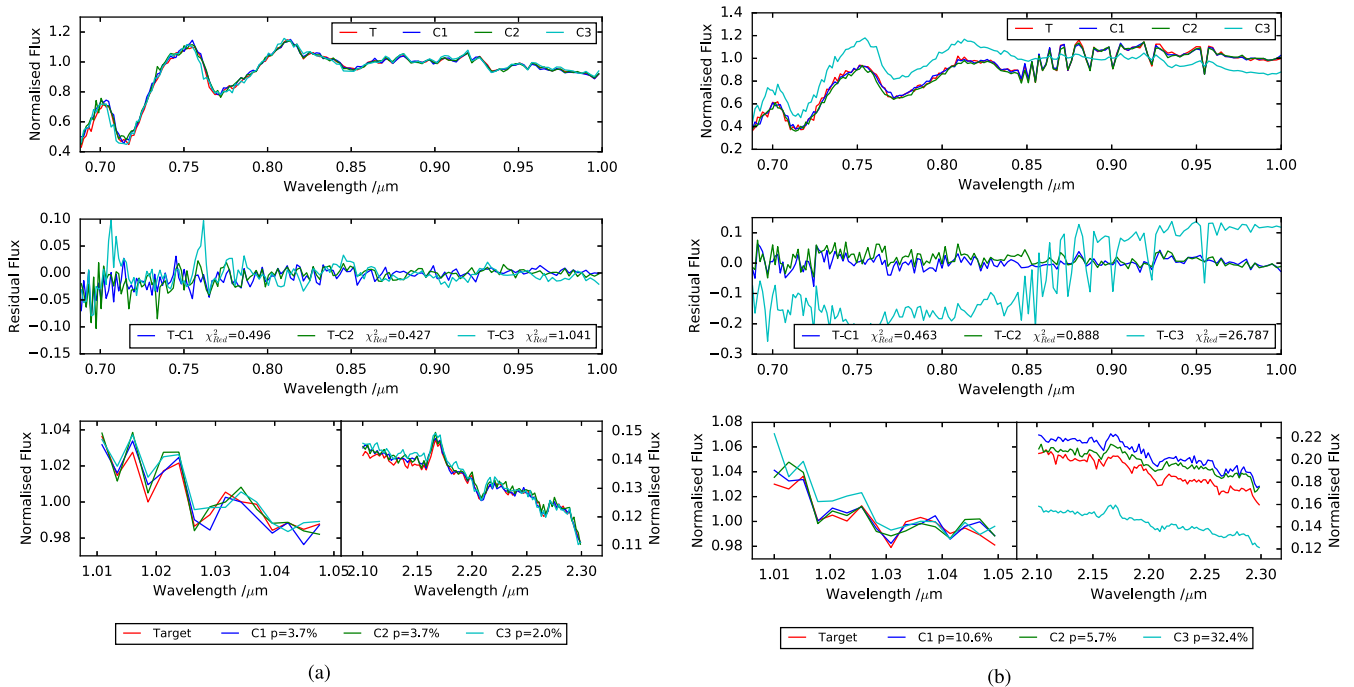| WISE ID	Group	Sub-group	α	δ	J [mag]	SpT	Date	t [min]	Airmass
J100449.01+135334.6	751	Control 2	10:04:49.01	+13:53:34.7	13.55	M3.5	2016/03/17	10.1	1.09
J095202.99+020820.5	751	Control 3	09:52:03.00	+02:08:20.6	12.66	M3.5	2016/03/17	2.8	1.22
J102115.33+422822.5	757	Target	10:21:15.33	+42:28:22.5	13.35	M3.5	2016/03/19	7.7	1.10
J101655.64+415752.6	757	Control 1	10:16:55.65	+41:57:52.6	13.00	M3.5	2016/03/19	4.1	1.12
J102402.03+374148.4	757	Control 2	10:24:02.04	+37:41:48.4	13.76	M3.5	2016/03/19	12.7	1.11
J103056.60+471237.9	757	Control 3	10:30:56.60	+47:12:38.0	13.55	M3.5	2016/03/19	10.0	1.21
J102051.15+474023.9	761	Target	10:20:51.16	+47:40:24.0	13.15	M3.5	2016/03/19	6.1	1.14
J103540.64+472827.4	761	Control 1	10:35:40.64	+47:28:27.4	13.99	M3.5	2016/03/19	17.1	1.14
J103236.96+455934.3	761	Control 2	10:32:36.96	+45:59:34.4	13.87	M3.5	2016/03/19	15.2	1.11
J095850.08+451018.8	761	Control 3	09:58:50.08	+45:10:18.8	12.89	M3.5	2016/03/19	3.7	1.13
J100202.50+074136.3	800	Target	10:02:02.51	+07:41:36.4	12.53	M3.5	2016/03/18	2.5	1.03
J100211.65+075540.6	800	Control 1	10:02:11.65	+07:55:40.6	13.40	M3.5	2016/03/18	8.3	1.03
J100515.21+110551.5	800	Control 2	10:05:15.21	+11:05:51.6	13.37	M3.5	2016/03/18	8.4	1.03
J101911.78+101143.2	800	Control 3	10:19:11.79	+10:11:43.3	12.59	M3.5	2016/03/18	2.6	1.03
J093819.44+565237.6	862	Target	09:38:19.45	+56:52:37.7	12.97	M4.0	2016/03/19	4.1	1.26
J092416.41+555952.1	862	Control 1	09:24:16.41	+55:59:52.2	13.16	M4.0	2016/03/19	5.6	1.24
J090223.85+620747.4	862	Control 2	09:02:23.85	+62:07:47.4	13.54	M4.0	2016/03/19	9.7	1.35
J092142.11+643630.5	862	Control 3	09:21:42.12	+64:36:30.6	12.12	M4.0	2016/03/19	2.1	1.49
J092547.70+430605.3	890	Target	09:25:47.71	+43:06:05.3	12.59	M4.0	2016/03/19	2.5	1.14
J100815.76+420546.1	890	Control 1	10:08:15.77	+42:05:46.1	13.49	M4.0	2016/03/19	8.9	1.20
J092438.33+383415.6	890	Control 2	09:24:38.33	+38:34:15.7	12.72	M4.0	2016/03/19	2.9	1.08
J091551.28+470403.7	890	Control 3	09:15:51.29	+47:04:03.7	12.94	M4.0	2016/03/19	3.9	1.13
J090908.53+354727.5	918	Target	09:09:08.53	+35:47:27.6	13.20	M3.5	2016/03/18	6.1	1.04
J090520.58+324153.3	918	Control 1	09:05:20.58	+32:41:53.4	14.05	M3.5	2016/03/18	18.7	1.03
J090322.79+394915.2	918	Control 2	09:03:22.79	+39:49:15.2	13.41	M3.5	2016/03/18	8.7	1.08
J093315.96+355255.4	918	Control 3	09:33:15.97	+35:52:55.5	13.38	M3.5	2016/03/18	8.2	1.05
J090114.01+331945.1	927	Target	09:01:14.01	+33:19:45.2	13.18	M4.0	2016/03/18	5.4	1.08
J092037.17+363745.6	927	Control 1	09:20:37.17	+36:37:45.7	13.96	M4.0	2016/03/18	17.3	1.10
J084240.19+262513.0	927	Control 2	08:42:40.19	+26:25:13.0	13.60	M4.0	2016/03/18	10.1	1.01
J093334.33+381013.3	927	Control 3	09:33:34.33	+38:10:13.3	13.44	M4.0	2016/03/18	9.1	1.07
J085410.72+443149.3	942	Target	08:54:10.72	+44:31:49.4	12.92	M3.5	2016/03/18	3.5	1.27
J084026.52+435854.7	942	Control 1	08:40:26.53	+43:58:54.8	13.74	M3.5	2016/03/18	13.7	1.21
J090549.19+482615.8	942	Control 2	09:05:49.19	+48:26:15.9	13.28	M3.5	2016/03/18	6.6	1.24
J080946.15+464349.0	942	Control 3	08:09:46.16	+46:43:49.1	13.38	M3.5	2016/03/18	9.2	1.13
J085237.84+431441.7	946	Target	08:52:37.84	+43:14:41.8	13.42	M4.0	2016/03/17	8.1	1.11
J092250.12+432738.6	946	Control 1	09:22:50.12	+43:27:38.7	12.97	M4.0	2016/03/17	4.3	1.10
J091453.37+443448.5	946	Control 2	09:14:53.37	+44:34:48.6	13.54	M4.0	2016/03/17	9.7	1.13
J090309.84+354215.1	946	Control 3	09:03:09.84	+35:42:15.1	13.51	M4.0	2016/03/17	9.2	1.10
J084819.77+430919.4	956	Target	08:48:19.77	+43:09:19.5	12.91	M3.5	2016/03/17	3.6	1.09
J091529.41+430447.0	956	Control 1	09:15:29.42	+43:04:47.0	13.82	M3.5	2016/03/17	12.5	1.10
J090408.84+383249.0	956	Control 2	09:04:08.85	+38:32:49.1	13.22	M3.5	2016/03/17	6.9	1.05
J085431.35+374703.4	956	Control 3	08:54:31.35	+37:47:03.4	13.40	M3.5	2016/03/17	9.0	1.06
J084530.09+192606.6	961	Target	08:45:30.09	+19:26:06.7	13.79	M3.5	2016/03/19	12.7	1.11
J084634.84+191526.0	961	Control 1	08:46:34.84	+19:15:26.0	13.75	M3.5	2016/03/19	11.9	1.09
J084536.83+183555.3	961	Control 2	08:45:36.83	+18:35:55.3	12.99	M3.5	2016/03/19	3.7	1.05
J084800.51+212638.8	961	Control 3	08:48:00.52	+21:26:38.9	13.89	M3.5	2016/03/19	14.7	1.02
J082443.15+044240.8	985	Target	08:24:43.16	+04:42:40.9	13.33	M3.5	2016/03/17	7.3	1.12
J081557.78+005921.6	985	Control 1	08:15:57.79	+00:59:21.6	13.71	M3.5	2016/03/17	10.7	1.08
J084042.24+081202.4	985	Control 2	08:40:42.25	+08:12:02.4	12.65	M3.5	2016/03/17	2.6	1.07
J084338.17+080419.0	985	Control 3	08:43:38.18	+08:04:19.1	13.70	M3.5	2016/03/17	11.5	1.04

1 compared to control 2 and control 3, control 2 compared to control 1 and control 3, etc.) on which to base our false positive count.

(3) Model minus control

For each group, we selected one of the control stars (at random) and added to its spectrum a known L2 UCD (Kelu-1, Burgasser 2007, flux-normalized appropriately). Spectral ratio differences and t-values were then calculated by treating these artificially generated M+UCD objects in the same way as the candidates (in the type 1 analysis), pairing them up with unaltered control stars from the group. This therefore allowed us to assess the expected results for the case where every analysed group had an L2 signature injected into the spectrum of its 'candidate M dwarf'. This therefore provides an assessment of how effectively the colour-similar control stars allow a known L2 signature to be uncovered through our analysis. As for the type 1 analysis, we could only carry this out for the 25 groups that had two or three usable control stars.

We chose to use a t-value of 1.75 to indicate possible detections. This is close to our minimal requirement and represented a good trade-off between identifying interesting candidates and minimizing false positives. Table 4 presents our t-values for all 25 candidate M+UCD systems considered here.

Figure 6. Example of (a) a clean group (where no control stars were rejected), and (b) a group where one control star is rejected. Top panel of each plot shows the optical part of the SpeX spectrum, middle panel shows the residuals between the target and control stars, bottom panels show the numerator and denominator region of the spectrum used to calculate the *Y/K* band spectral ratio for both target and control stars, where we normalize the mean flux of the numerator to unity. The simulated cases use the same spectra as Fig. 4. T here is the target (M+UCD candidate), and C1, C2 and C3 are the control stars (for each observation group).

7 RESULTS AND DISCUSSION

We first consider the four targets whose t-values are greater than 1.75, and look more closely for potential signatures of unresolved UCD companions. The most interesting candidate is WISE J100202.50+074136.3, which was analysed as part of group 800 and yielded a t-value of 7.28. The spectral residuals and spectral ratio difference histograms for this group are shown in Fig. 7a. The residuals show a distinct maximum across the 1–1.3 μm range (i.e. the region covered by our selected spectral ratio difference bands), and this maximum appears to be significantly greater than the level of scatter we might expect in the absence of a near-infrared excess. In the 1.3–1.8 μm range, an excess signal is less clear, but may be present at a lower level. We also note a dip in the residuals at either end of this wavelength range, which is consistent with early L morphology. At longer wavelengths, any excess signal is lower still, but may be present when compared to the null case residuals. Overall the residuals are reasonably consistent with an early L dwarf across the full spectral range, and the significance of the 1–1.3 μm signal is born out in the spectral ratio difference histogram that shows the M+UCD candidate minus control values are well separated from the population of control star minus control star values. In contrast, Fig. 7b shows similar plots for a clear non-detection in our sample (WISE J140145.91+310640.6, part of group 228, t-value = −0.54). The mass of an ∼L0 companion to WISE J1002+0741 would depend on the age of the system. The latest BT-Settl models (Baraffe et al. 2015) suggest that for ages from ∼0.6–2 Gyr the object would have a mass close to the hydrogen burning mass limit, and for older or younger ages, it would be stellar or sub-stellar, respectively. Age constraints are not currently available for WISE J1002+0741 however.

Our other three possible detections come in two types. One (WISE J143046.74+272058.2, part of group 159) shows no apparent red residuals despite a significant t-value. Examination of the residual trace in the spectral ratio bands suggests that this t-value has been spuriously inflated by noise fluctuations and/or telluric absorption. The other two (WISE J104507.41+181311.0, part of group 697, and WISE J150642.41+324609.9, part of group 109) show significant red residuals, but of a somewhat different morphology to WISE J100202.50+074136.3. Fig. 8a shows the red residuals for the first of these candidates as an example, and these residuals peak around a wavelength of 1.6 μm, falling off on either side. In Fig. 8b, we provide a comparison spectral residual from our type 2 (control star minus control star) analysis. This residual signal was the only one from our type 2 analysis to yield a t-value >1.75, and is thus our best available example of a false positive. We note significant similarity between the example candidate (Fig. 8a) and the false positive (Fig. 8b), both of which have excess morphology that peaks around 1.6 μm. It thus seems likely WISE J104507.41+181311.0 and WISE J150642.41+324609.9 do not have unresolved UCD companions, although the excess flux (seen in their residual spectra) may well be genuine but with a different origin.

In order to broadly assess ultracool companionship and contamination in our full target sample, we now discuss the outcome of the three different types of analysis discussed in Section 6. Fig. 9 shows the percentages of M dwarfs with t-values greater than a range of different levels. The red, green and blue symbols/lines are for type 1, 2 and 3 analysis (i.e. t-values calculated from spectral ratio differences between M+UCD candidate and control star pairs, pairs of control stars, and model candidate and control star pairs). It is clear from the green symbols our method only identifies false positive

Table 3. Rejection table for our colour-similar control stars. Those control stars in bold were rejected as having either $\chi^2_{\rm Red} > 5$ (where the chi-squared fit is a comparison of the optical, < 1 μm, part of the target and control spectra) or Y/K $> 2\sigma$ (a comparison between the similarity of the target and control using a spectral ratio with bands 1.01–1.05 μm and 2.10–2.30 μm). Note Group 7 only had two control stars observed due to time constraints.

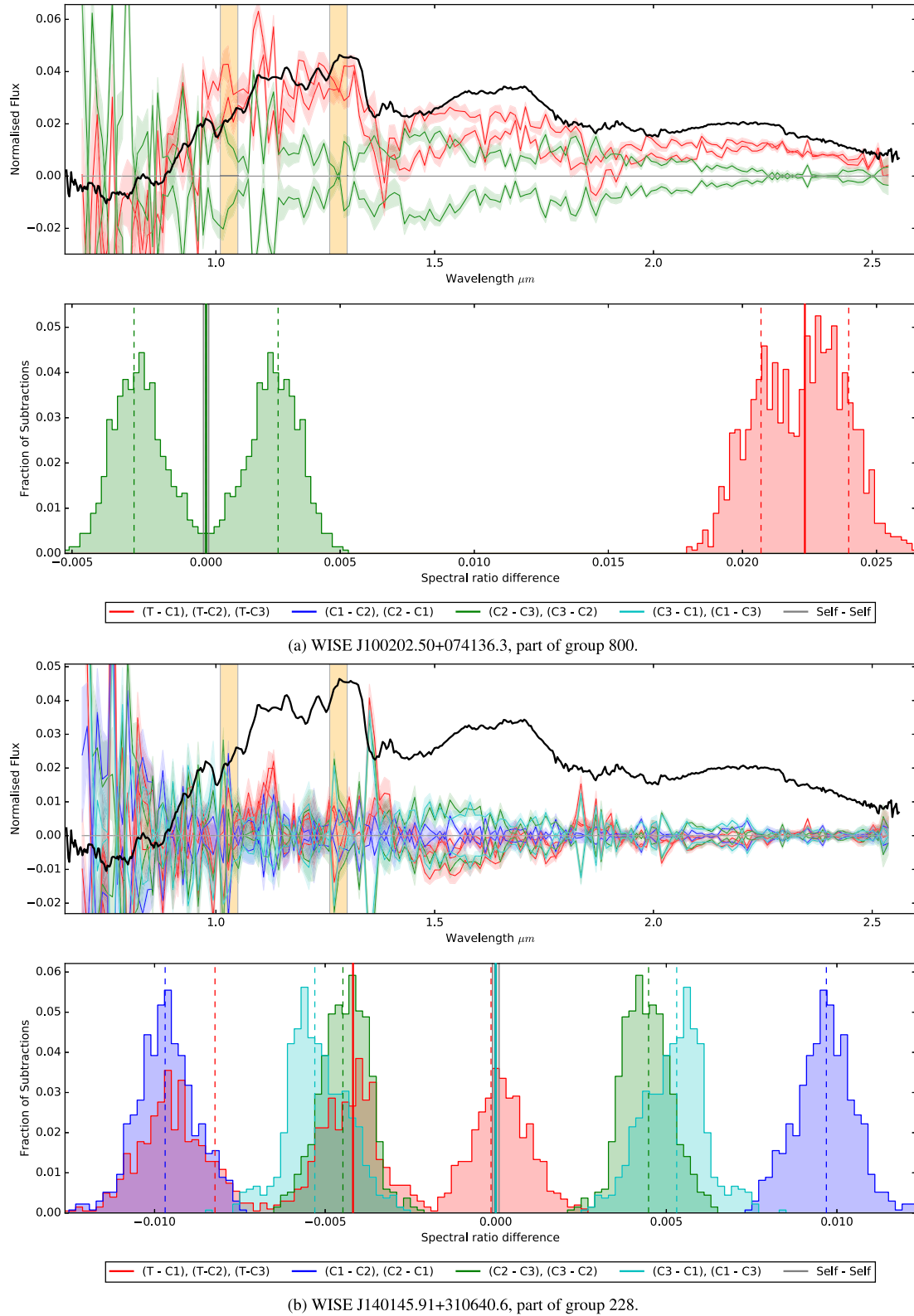| Group number	Control 1 $\chi^2_{\rm Red}$	YK per cent	Control 2 $\chi^2_{\rm Red}$	YK per cent	Control 3 $\chi^2_{\rm Red}$	YK per cent
7	0.55	6.3	0.66	4.6		
68	0.59	10.2	0.98	1.7	0.69	2.5
92	1.87	9.3	0.67	3.6	1.17	0.9
109	3.6	5.2	2.47	7.0	**10.45**	**16.8**
124	**1.68**	**17.6**	1.04	10.0	**0.55**	**11.4**
159	0.48	0.8	**1.1**	**15.1**	0.65	6.1
228	0.5	3.7	0.43	3.7	1.04	2.0
232	0.46	10.6	0.89	5.7	**26.79**	**32.4**
282	0.53	7.7	0.5	5.0	**0.62**	**11.9**
340	**4.3**	**13.1**	1.2	3.4	0.77	6.8
360	0.53	5.4	0.45	2.1	0.47	1.4
466	0.69	3.6	0.63	0.7	0.67	1.6
476	**2.23**	**15.5**	**1.19**	**12.1**	0.8	6.3
550	2.02	8.7	0.81	4.3	1.17	2.7
697	0.92	1.9	1.02	5.0	**24.71**	**26.0**
751	1.23	4.8	0.69	2.0	0.69	0.6
757	0.98	9.7	0.73	6.0	1.36	6.3
761	0.49	3.6	0.98	3.7	2.12	5.2
800	**2.5**	**12.0**	2.32	2.6	1.02	4.2
862	1.11	0.1	0.88	4.2	1.49	1.0
890	1.3	1.3	0.8	9.7	0.93	3.8
918	0.61	2.5	1.09	1.8	0.87	1.6
927	**0.61**	**11.8**	**1.25**	**13.1**	**2.1**	**13.3**
942	0.65	8.6	0.75	2.5	**1.2**	**13.9**
946	0.66	2.9	0.53	1.5	1.01	0.9
956	0.56	0.7	0.62	0.4	0.75	5.6
961	0.35	2.1	0.4	0.0	0.45	2.9
985	0.39	2.1	0.53	5.4	0.59	2.4

Table 4. The resulting t-values for all observations. $T - C$ is target minus control subtractions, $M - C$ is the subtractions where a control star (to which a UCD has been added) is subtracted from the other control stars, and $CX - C$ is the subtractions of one control star (chosen as the target) minus the other control stars. In bold are those that we indicate as possible detections (t-value > 1.75).

Group	$T - C$	$M - C$	$C1 - C$	$C2 - C$	$C3 - C$
7	0.99	**2.73**	–	–	–
68	−0.39	**2.08**	0.01	1.25	−1.33
92	0.12	0.37	−4.13	0.64	0.29
109	**6.44**	**6.75**	–	–	–
159	**6.61**	**6.36**	–	–	–
228	−0.54	1.45	1.51	−1.3	−0.03
232	−5.83	**2.94**	–	–	–
282	1.59	1.24	–	–	–
340	1.63	1.38	–	–	–
360	−2.1	**2.74**	−0.12	1.55	−1.01
466	−0.05	1.28	−2.86	0.22	0.71
550	0.49	1.56	−0.53	−0.36	**8.03**
697	**2.09**	**1.76**	–	–	–
751	0.44	1.05	−5.99	0.4	0.42
757	−1.1	1.15	1.32	0.02	−1.46
761	−0.47	0.73	0.81	−2.39	0.18
800	**7.28**	**3.43**	–	–	–
862	0.69	0.78	−1.17	1.46	−0.04
890	−2.3	**5.12**	−0.05	−0.87	1.31
918	−0.19	0.42	−8.71	0.56	0.36
942	0.16	0.79	–	–	–
946	0.36	**2.25**	0.85	−1.86	0.27
956	0.12	−0.52	0.23	0.69	−3.63
961	−0.5	0.51	−6.72	0.36	0.56
985	−0.57	0.77	0.31	−3.61	0.63

signals around a small fraction of our control star pairings (just one with a t-value > 1.75). However, this signal can have quite a high significance, and may well represent a genuine excess albeit not due to an unresolved UCD companion. The blue symbols show if every M dwarf had an unresolved UCD companion, then they would manifest as a range of t-values, more numerous for lower values, and with an expected yield of $\sim$40 per cent with a t-value > 1.75. The red symbols lie about mid-way between the blue and green for t-values < 3.5, but lie close to the blue symbols (and well above the green symbols) for higher values. We loosely interpret this as being consistent with an intermediate percentage of unresolved UCD companions, some fraction of which should have t-value > 1.75, combined with several times the number of false positives present amongst the control stars. This is roughly consistent with the results suggested by our spectral residual inspection (i.e. we have one good unresolved UCD candidate and three probable false positives).

We have considered a variety of possible effects that might lead to false positive signatures amongst our candidates, and estimated their likelihood and/or expected levels of occurrence.

Intrinsic properties of the target M dwarf systems are an important consideration. M dwarf variability could lead to an apparent mid-infrared (MIR) photometric excess (leading to an M dwarf being selected in our Paper I analysis), and if such variability is due to spots and rotation, then this might also affect their spectra, e.g. high level spot coverage could lead to a spectrum consisting of warmer (photospheric) and cooler (from spots) components. How-
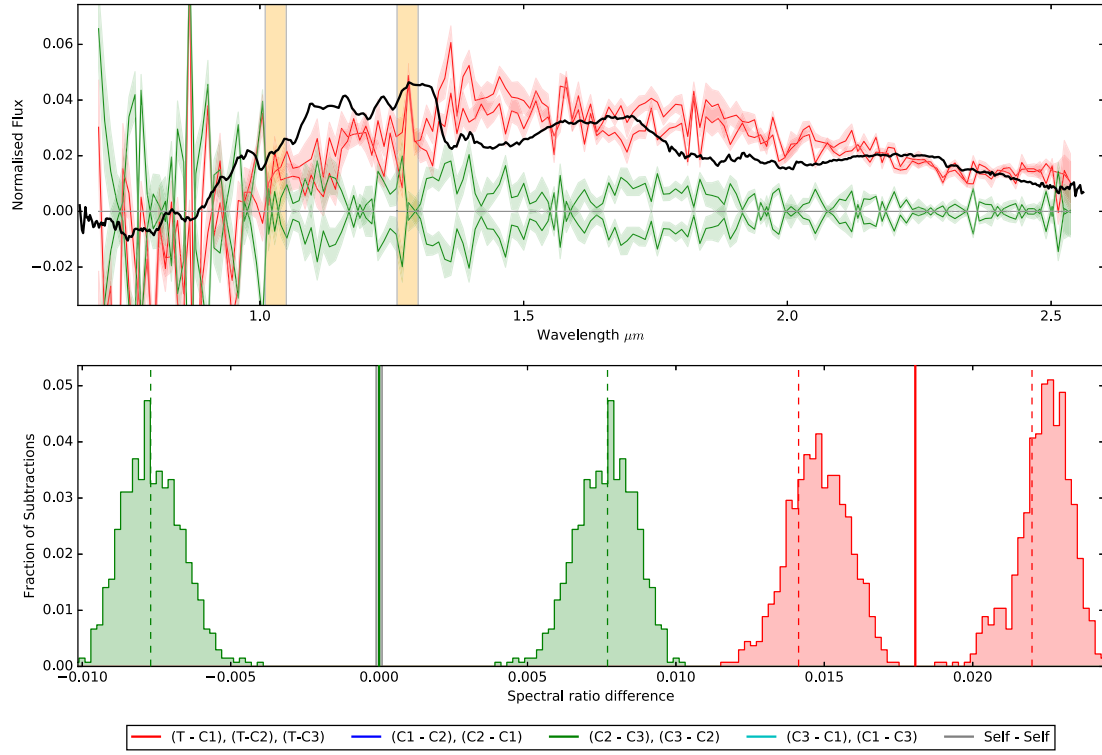
ever, our Paper I analysis established the M+UCD candidates are not significantly variable on time-scales of hours to days. In any event, photosphere/spot temperature differentials for M dwarf spots are of order $\sim$150 K (Vida et al. 2016) and thus unlikely to mimic the signature of an unresolved UCD companion. An unresolved M (non-UCD) companion could lead to low-level differences between a candidate and a single M dwarf control star; however, the residual spectra would not resemble a UCD and the resulting MIR excess would be negligible. The presence of dusty discs around M dwarfs could cause an MIR excess; however, an NIR/MIR multicolour analysis of our candidate sample (Appendix A1) indicates there are no obvious discs present that could account for the unresolved companion signatures.

Chance alignments, where background/foreground objects are blended with the candidates, could produce MIR excess and affect the NIR spectral shape. However, we have estimated likely levels of such alignments (Appendices A2–A5) and expect no more than 0.1 per cent due to galactic sources (cooler M dwarfs, M giants and brown dwarfs), and a worst case scenario of 8–9.5 per cent due to red galaxies. Indeed, a random-offset-analysis suggests an $\sim$3.5 per cent level of chance alignments with sufficient excess to be mistaken for a UCD (Appendix A6). We also note we have visually inspected candidates in *WISE*, 2MASS, SDSS and where possible in UKIDSS and DSS2 (Appendix A7) to rule out source blending as much as possible. While low level of blending may remain (causing the MIR excess of some candidates), any resulting NIR excess would not be expected to resemble UCD morphology.
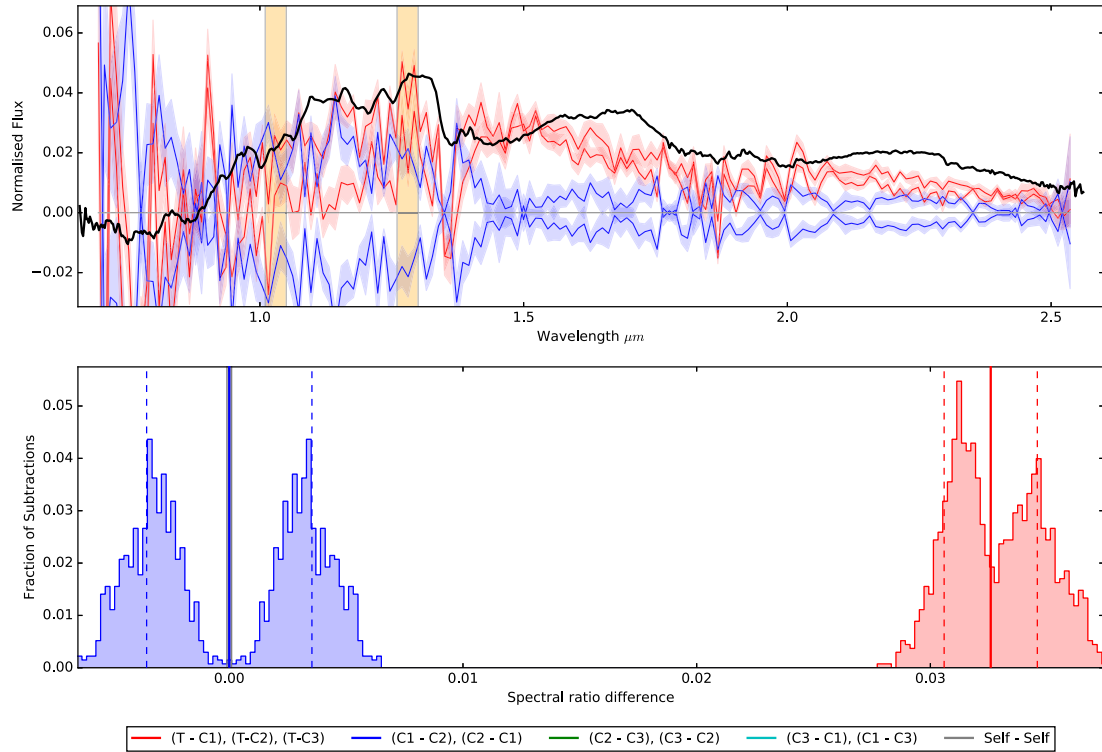
We also modelled the effects in residual spectra using M dwarf pairings with slightly different properties (to see if false positives could be generated in the absence of a UCD companion).

(a) WISE J100202.50+074136.3, part of group 800.

(b) WISE J140145.91+310640.6, part of group 228.

Figure 7. Layout identical to Fig. 4. (a) An example of a target minus control subtraction, one of our M+UCD candidates for which a spectroscopic signature of a UCD was found (t-value = 7.8) where one control star was rejected. (b) An example of a non-detection (t-value ~0.0) where no control stars were rejected. Plotted in black is a comparison L0 residual (M4 is LP 508-14, Burgasser et al. 2004, and the L0 is 2MASP J0345432+254023, Burgasser & McElwain 2006).

(a) WISE J104507.41+181311.0, part of group 697.

(b) WISE J115522.06+002657.3, part of group 550.

Figure 8. Layout identical to Fig. 4. (a) An example of target minus control subtraction, showing significant red residuals but of a somewhat different morphology to WISE J100202.50+074136.3. (b) An example control minus control subtraction; this residual signal was the only one from our our type 2 analysis to yield a t-value >1.75. Plotted in black is a comparison L0 residual (M4 is LP 508-14, Burgasser et al. 2004, and the L0 is 2MASP J0345432+254023, Burgasser & McElwain 2006).

Figure 9. Percentage of groups yielding a detected unresolved UCD signature as a function of t-value threshold. The three types of analysis [M+UCD candidate minus control star, control star minus control star and model candidate minus control star (see Section 6)] are shown as red, green and blue symbols, respectively.

Using 75 PHOENIX synthetic spectra (Husser et al. 2013) with combination of $T_{\rm eff}$ (2800, 2900, 300, 3100, 3200 K), log *g* (4.5, 5.0, 5.5) and [Fe/H] (-1, -0.5, 0, 0.5, 1), we generated 5500 residual spectra that were subjected to our M+UCD candidate analysis procedures. Of these, 884 (16 per cent) passed the spectral similarity criteria ($\chi^2_{\rm Red} > 5$ or Y/K $> 2\sigma$) and 417 (7.6 per cent) yielded t-values greater than 1.75. However, the relative ($J - W2$) excess between these pairings was in the range 0.002 ± 0.026 (3σ), well below the level required to be selected as M+UCD candidates in the first place. By comparison, WISE J100202.50+074136.3 has a relative ($J - W2$) excess of 0.093 mag and our full M+UCD candidate sample has a minimum excess of $\sim$0.045 mag (see Paper I).

Overall this analysis suggests an expected NIR excess rate of 3.5–9.5 per cent, due mainly to blended background galaxies. This compares favourably with the two candidates we identify as probably false positives in our analysis (showing NIR excess in their residual spectra, but with non-UCD-like morphology). We have not found a good alternative explanation for WISE J100202.50+074136.3, and consider it to be a strong M+UCD candidate.

Using the results from our first follow-up sample, we estimated the occurrence rate of unresolved UCD companions to M dwarfs in our full candidate sample, as well as the potential 'catch' that would result from comprehensive follow-up. Based on our assessment, our sample contains one unresolved UCD companion and three false positives, combined with an approximate recovery rate of $\sim$40 per cent (from the model candidate and control star results in Fig. 8) we estimate an occurrence rate of $\frac{1}{24 \times 0.4} \sim 0.1$. This is substantially higher than the expected occurrence rate for a randomly selected sample of M dwarfs, and although this is based on just one good candidate, it suggests our candidate selection method (from paper I) may be achieving its desired goal. If this occurrence rate is appropriate for our full excess sample of 1082 candidates, then we might expect up to $\sim$100 unresolved UCD companions within

the sample, and the potential to recover $\sim$40 of these through an expanded spectroscopic follow-up campaign (cf. Fig. 1, where only a handful of such M3–M5 companions are known).

8 CONCLUSIONS

We have developed a spectroscopic method to identify the signatures of unresolved L dwarf companions to mid-M dwarfs, with targets and their associated optically colour-similar control stars coming from the photometric analysis of Paper I. As a first stage, our method makes use of spectral ratio differences between the spectra of candidates and their control stars, which mitigates against the scatter in M dwarf colours (and spectral morphology) that occurs across the full population for any particular M spectral type. As a second stage, our method examines spectral difference residuals (between candidate and control star pairings), to visually reveal any near-infrared excess flux from ultracool companions. Testing showed our spectroscopic method is optimized by spectral ratio differences in the 1.21–1.35 μm and 0.96–1.10 μm bands, and the best near-infrared spectroscopy for this purpose should have a spectral resolution of $\sim$200 and a signal to noise of $\sim$125–200.

We obtained a suitable data set for a pilot sample from Paper I during good conditions with SpeX on the IRTF. The identification of the strong signature for WISE J100202.50+074136.3 (($J - W2$) excess of 0.093), was recognized with a t-value of 7.28 and showed early L-like morphology in the residual spectra, is encouraging and should be followed up. Adaptive optics should be capable of resolving a companion at separations >0.1 arcsec (>15 au at the M dwarf distance of 150 pc), and radial velocity variations[3] (of at least $\sim$3 km s^{-1}) would be expected for separations out to $\sim$1 au (with periods ranging up to $\sim$2 yr). Also, *Gaia* (during its 5 yr mission) may detect an astrometric wobble of several milli arcsec amplitude for separations out to $\sim$3 au. Thus direct/indirect detection of this candidate companion may be eminently possible with current facilities. And with full follow-up of our candidate sample from Paper I, we might expect to confirm up to $\sim$40 such companions in the future, adding extensively to the known desert population of M3–M5 dwarfs.

---

[3] Calculated online at http://astro.unl.edu/classaction/animations/extrasolarplanets/radialvelocitysimulator.html

REFERENCES

Adams F. C., Hollenbach D., Laughlin G., Gorti U., 2004, ApJ, 611, 360
Armitage P. J., Bonnell I. A., 2002, MNRAS, 330, L11
Astropy Collaboration et al., 2013, A&A, 558, A33
Baraffe I., Homeier D., Allard F., Chabrier G., 2015, A&A, 577, A42
Beckwith S. V. W., Sargent A. I., Chini R. S., Guesten R., 1990, AJ, 99, 924
Blanton M. R., Roweis S., 2007, AJ, 133, 734
Boylan-Kolchin M., Springel V., White S. D. M., Jenkins A., Lemson G., 2009, MNRAS, 398, 1150
Burgasser A. J., 2007, ApJ, 658, 617
Burgasser A. J., McElwain M. W., 2006, AJ, 131, 1007
Burgasser A. J., McElwain M. W., Kirkpatrick J. D., Cruz K. L., Tinney C. G., Reid I. N., 2004, AJ, 127, 2856
Burgasser A. J., Kirkpatrick J. D., Cruz K. L., Reid I. N., Leggett S. K., Liebert J., Burrows A., Brown M. E., 2006, ApJS, 166, 585
Burgasser A. J., Liu M. C., Ireland M. J., Cruz K. L., Dupuy T. J., 2008, ApJ, 681, 579
Burgasser A. J., Cruz K. L., Cushing M., Gelino C. R., Looper D. L., Faherty J. K., Kirkpatrick J. D., Reid I. N., 2010, ApJ, 710, 1142
Burningham B. et al., 2013, MNRAS, 433, 457
Burrows A., Hubbard W. B., Lunine J. I., Liebert J., 2001, Rev. Mod. Phys., 73, 719
Calvet N., Hartmann L., Strom S. E., 2000, in Mannings V., Boss A. P., Russell S. S., eds, Protostars and Planets IV. Univ. Arizona Press, Tucson, AZ, p. 377
Chabrier G., Gallardo J., Baraffe I., 2007, A&A, 472, L17
Chabrier G., Johansen A., Janson M., Rafikov R., 2014, in Beuther H., Klessen R. S., Dullemond C. P., Henning T., eds, Protostars and Planets IV. Univ. Arizona Press, Tucson, AZ, p. 619
Cheetham A. C., Kraus A. L., Ireland M. J., Cieza L., Rizzuto A. C., Tuthill P. G., 2015, ApJ, 813, 83
Choi M., Tatematsu K., Kang M., 2010, ApJ, 723, L34
Choquet É. et al., 2016, ApJ, 817, L2
Cook N. J. et al., 2016, MNRAS, 457, 2192 (Paper I)
Covey K. R., West A. A., Bochanski J. J., Hawley S. L., 2014, Astrophysics Source Code Library, record ascl:1405.003
Cruz K. L. et al., 2007, AJ, 133, 439
Csizmadia S. et al., 2015, A&A, 584, A13
Cui X.-Q. et al., 2012, Res. Astron. Astrophys., 12, 1197
Cushing M. C., Vacca W. D., Rayner J. T., 2004, PASP, 116, 362

De Lee N. et al., 2013, AJ, 145, 155
Deacon N. R., Schlieder J. E., Olofsson J., Johnston K. G., Henning T., 2013, MNRAS, 434, 1117
Dieterich S. B., Henry T. J., Golimowski D. A., Krist J. E., Tanner A. M., 2012, AJ, 144, 64
Duquennoy A., Mayor M., 1991, A&A, 248, 485
Dutrey A., Guilloteau S., Duvert G., Prato L., Simon M., Schuster K., Menard F., 1996, A&A, 309, 493
Eiroa C. et al., 2013, A&A, 555, A11
Esplin T. L., Luhman K. L., Mamajek E. E., 2014, ApJ, 784, 126
Gizis J. E., Kirkpatrick J. D., Burgasser A., Reid I. N., Monet D. G., Liebert J., Wilson J. C., 2001, ApJ, 551, L163
Guo Q. et al., 2011, MNRAS, 413, 101
Halbwachs J. L., Mayor M., Udry S., Arenou F., 2003, A&A, 397, 159
Han C. et al., 2016, ApJ, 822, 75
Henriques B. M. B., White S. D. M., Lemson G., Thomas P. A., Guo Q., Marleau G.-D., Overzier R. A., 2012, MNRAS, 421, 2904
Hinkley S. et al., 2015, ApJ, 806, L9
Husser T.-O., Wende-von Berg S., Dreizler S., Homeier D., Reiners A., Barman T., Hauschildt P. H., 2013, A&A, 553, A6
Jarrett T. H. et al., 2011, ApJ, 735, 112
Jones E. et al., 2001, SciPy: Open Source Scientific Tools for Python. Available at: http://www.scipy.org/
Jordi K., Grebel E. K., Ammon K., 2006, A&A, 460, 339
Jumper P. H., Fisher R. T., 2013, ApJ, 769, 9
Kirkpatrick J. D. et al., 2010, ApJS, 190, 100
Kraus A. L., Ireland M. J., Martinache F., Hillenbrand L. A., 2011, ApJ, 731, 8
Lawrence A. et al., 2007, MNRAS, 379, 1599
Lawrence A. et al., 2013, VizieR Online Data Catalog, 2319
Lépine S., Hilton E. J., Mann A. W., Wilde M., Rojas-Ayala B., Cruz K. L., Gaidos E., 2013, AJ, 145, 102
Lestrade J.-F., Wyatt M. C., Bertoldi F., Menten K. M., Labaigt G., 2009, A&A, 506, 1455
Li Y., Kouwenhoven M. B. N., Stamatellos D., Goodwin S. P., 2015, ApJ, 805, 116
Luhman K. L., Mamajek E. E., 2012, ApJ, 758, 31
Luo A.-L., Zhang Y.-X., Zhang J.-N., Zhao Y.-H., 2004, in Quinn P. J., Bridger A., eds, Proc. SPIE Conf. Ser. Vol. 5493, Optimizing Scientific Return for Astronomy through Information Technologies. SPIE, Bellingham, p. 178
Luo A.-L. et al., 2012, Res. Astron. Astrophys., 12, 1243
Ma B., Ge J., 2014, MNRAS, 439, 2781
McCarthy C., Zuckerman B., 2004, AJ, 127, 2871
Marcy G. W., Butler R. P., 2000, PASP, 112, 137
Marocco F. et al., 2015, MNRAS, 449, 3651
Mawet D. et al., 2015, ApJ, 811, 103
Murillo N. M., Lai S.-P., Bruderer S., Harsono D., van Dishoeck E. F., 2013, A&A, 560, A103
Naab T., Johansson P. H., Ostriker J. P., 2009, ApJ, 699, L178
Pérez F., Granger B. E., 2007, Comput. Sci. Eng., 9, 21
Phan-Bao N. et al., 2003, A&A, 401, 959
Phan-Bao N. et al., 2008, MNRAS, 383, 831
Plavchan P., Werner M. W., Chen C. H., Stapelfeldt K. R., Su K. Y. L., Stauffer J. R., Song I., 2009, ApJ, 698, 1068
Rayner J. T., Toomey D. W., Onaka P. M., Denault A. J., Stahlberger W. E., Vacca W. D., Cushing M. C., Wang S., 2003, PASP, 115, 362
Reid I. N., Cruz K. L., Allen P. R., 2007, AJ, 133, 2825
Robin A. C. et al., 2012, A&A, 543, A100
Roeser S., Demleitner M., Schilbach E., 2010, AJ, 139, 2440
Ryden B., Partridge B., 2004, Introduction to Cosmology, Vol. 57. Addison-Wesley, Boston
Skrutskie M. F. et al., 2006, AJ, 131, 1163
Smart R. L., 2016, Astron. Comput., 15, 29
Spitzer L., 1978, Physical Processes in the Interstellar Medium. Wiley, New York
Springel V. et al., 2005, Nature, 435, 629

Stamatellos D., Whitworth A. P., 2009, MNRAS, 392, 413

Straižys V., Lazauskaitė R., 2009, Balt. Astron., 18, 19

Taylor M. B., 2005, in Shopbell P., Britton M., Ebert R., eds, ASP Conf. Ser. Vol. 347, Astronomical Data Analysis Software and Systems XIV. Astron. Soc. Pac., San Francisco, p. 29

Taylor M. B., 2006, in Gabriel C., Arviset C., Ponz D., Enrique S., eds, ASP Conf. Ser. Vol. 351, Astronomical Data Analysis Software and Systems XV. Astron. Soc. Pac., San Francisco, p. 666

Theissen C. A., West A. A., 2014, ApJ, 794, 146

Tobin J. J., Hartmann L., Chiang H.-F., Wilner D. J., Looney L. W., Loinard L., Calvet N., D'Alessio P., 2012, Nature, 492, 83

Vacca W. D., Cushing M. C., Rayner J. T., 2003, PASP, 115, 389

van der Plas G. et al., 2016, ApJ, 819, 102

Vida K. et al., 2016, A&A, 590, A11

Weisstein E. W., 1999, Spherical Cone. From MathWorld–A Wolfram Web Resource. Available at: http://mathworld.wolfram.com/SphericalCone.html

Wenger M. et al., 2000, A&AS, 143, 9

Whitworth A. P., Stamatellos D., 2006, A&A, 458, 817

Wilson P. A. et al., 2016, A&A, 588, A144

Wright E. L. et al., 2010, AJ, 140, 1868

York D. G. et al., 2000, AJ, 120, 1579

Zhao G., Zhao Y.-H., Chu Y.-Q., Jing Y.-P., Deng L.-C., 2012, Res. Astron. Astrophys., 12, 723

Zhong J. et al., 2015, AJ, 150, 42

APPENDIX A: CONTAMINATION IN THE EXCESS SAMPLE AND CANDIDATE M+UCDS

A1 Contamination from discs

Circumstellar discs around M dwarfs can be approximated quite well by a blackbody of temperature, T_{eff} and of extent R. These discs are heated by the central star and as such cannot exceed the stellar temperature unless some other process is involved. One way discs are found is to look for MIR excess (for M dwarfs e.g. Esplin, Luhman & Mamajek 2014, Theissen & West 2014 and Luhman & Mamajek 2012).

Esplin et al. (2014) investigate the excess signal via MIR continuum emission from warm circumstellar dust. They define a boundary (see fig. 2 from Esplin et al. 2014) above which stars have an excess signal due to this warm dust. Theissen & West (2014) compliment this with a polynomial fit (see table 1, Theissen & West 2014) to the M dwarf main sequence with $(W1 - W3)$ and $(W2 - W3)$ as functions of $(r - z)$ from SDSS. Our M dwarfs lie well below the region in which M dwarfs are known to have circumstellar discs lie (fig. 3 from Theissen & West 2014), and mostly lie out of the region defined by Esplin et al. (2014). Luhman & Mamajek (2012) also present a boundary in $(K_S - W2)$ colour-spectral type space; however, their boundaries lie significantly above our distribution and the boundary of Esplin et al. (2014), thus having no overlap with our M+UCD candidates.

To investigate the effects of circumstellar reddening further, we investigated ways in which warm discs (of various size) might give excess values that could contaminate our selection of M+UCD candidates.

$$B_\lambda = \frac{2hc^2}{\lambda^5} \frac{1}{\exp(hc/\lambda k_B T_{eff}) - 1}$$

$$F_\lambda = \pi B_\lambda$$

$$F_\lambda(d) = F_\lambda \frac{\Sigma_{disc}}{\Sigma_{sphere}} \tag{A1}$$

where B_λ is the spectral radiance, F_λ is the flux, $F_\lambda(d)$ is the flux as observed from a distance d, $\Sigma_{disc} = \pi(R_{outer}^2 - \pi R_{inner}^2)$ is the surface area of the disc with inner radius R_{inner} and outer radius R_{outer} and $\Sigma_{sphere} = 4\pi d^2$ is the surface area of a sphere at radius d, the distance of observation (taken to be 10 pc).

We made a grid of 250 values of $0.5 < \log(\frac{T_{eff}}{K}) < 3.6$ and 250 values of $-3.5 < \log(\frac{extent\ of\ disc}{au}) < 4.5$ (where extent of disc $\approx R_{outer}$ as we set $R_{inner} = R_*$). From these 62 500 T_{eff} and extent of disc combinations, we added a blackbody as described in equation (A1) to the M dwarf BT-Settl (CIFIST2011_2015, Baraffe et al. 2015)[4] model (smoothed to 5000 bins for faster computation between 0 and 30 μm, and normalized to 10 pc). For each point in the grid, the colour excess (Colour$_{M + disc}$ − Colour$_{Mdwarf}$) was calculated for $(J - H)$, $(H - W1)$, $(H - W2)$, $(J - W1)$, $(J - W2)$ and $(W2 - W3)$ where colour is calculated in equation (A2).

Colour$(1, 2) = M_1 - M_2$

$$= -2.5\log_{10}\left(\frac{\int I_\lambda \tau_1(\lambda)d\lambda}{\int I_{0,1}\tau_1(\lambda)d\lambda} \frac{\int I_{0,2}\tau_2(\lambda)d\lambda}{\int I_\lambda \tau_2(\lambda)d\lambda}\right) \tag{A2}$$

where I_λ is the flux from the spectrum, $\tau_1(\lambda)$ is the transmission profile of band 1 and $I_{0,1}$ is the zero-point flux of band 1.[5]

To these grids, we added data from the literature for known circumstellar discs, CSD, debris discs, DD, around low-mass stars (from Plavchan et al. 2009; Eiroa et al. 2013; Choquet et al. 2016) protostellar discs, PSD, around low-mass stars (from Choi et al. 2010; Tobin et al. 2012; Murillo et al. 2013), low-mass T-Tauri stars, TT (from Dutrey et al. 1996) and from the Solar system (Asteroid belt, Kuiper belt and Oort cloud). We also added some models of debris discs from Lestrade et al. (2009) for M0, M3 and M6 dwarfs; a model of accretion discs from Calvet et al. (2000), models of circumstellar discs for M3–M8 dwarfs from van der Plas et al. (2016), a model of gas escape velocity from Adams et al. (2004), a model of PSD and protoplanetary discs, PPD from Chabrier et al. (2014) and a model of radiative equilibrium for small particles by Beckwith et al. (1990) and Spitzer (1978).

We used these to show how much colour excess at given T_{eff} and extent would add to an M dwarf assuming they were blackbodies. Fig. A1 shows these grid points plotted for an M4 dwarf with the comparison to the literature.

As a red $(W2 - W3)$ colour is a clear signature of a disc, we also plotted $(W2 - W3)$ against colour excess in $(J - W2)$ for all our M dwarfs in the full M dwarf candidate catalogue with a $W3$ detection (non-upper limit) and for our M+UCD candidates that have a $W3$ detection (see Fig. A2). Fig. A2 shows there are no major outliers and therefore no obvious discs present in our M+UCD candidates.

In addition to this analysis, discs around late-K and M dwarfs seem to be rare and only present around young M dwarfs (see Deacon et al. 2013, and references therein). Even if these rare discs exist from work presented above, it is clear only exceptionally warm or large discs would give the colour excess required to be mistaken for one of our M+UCD candidates.
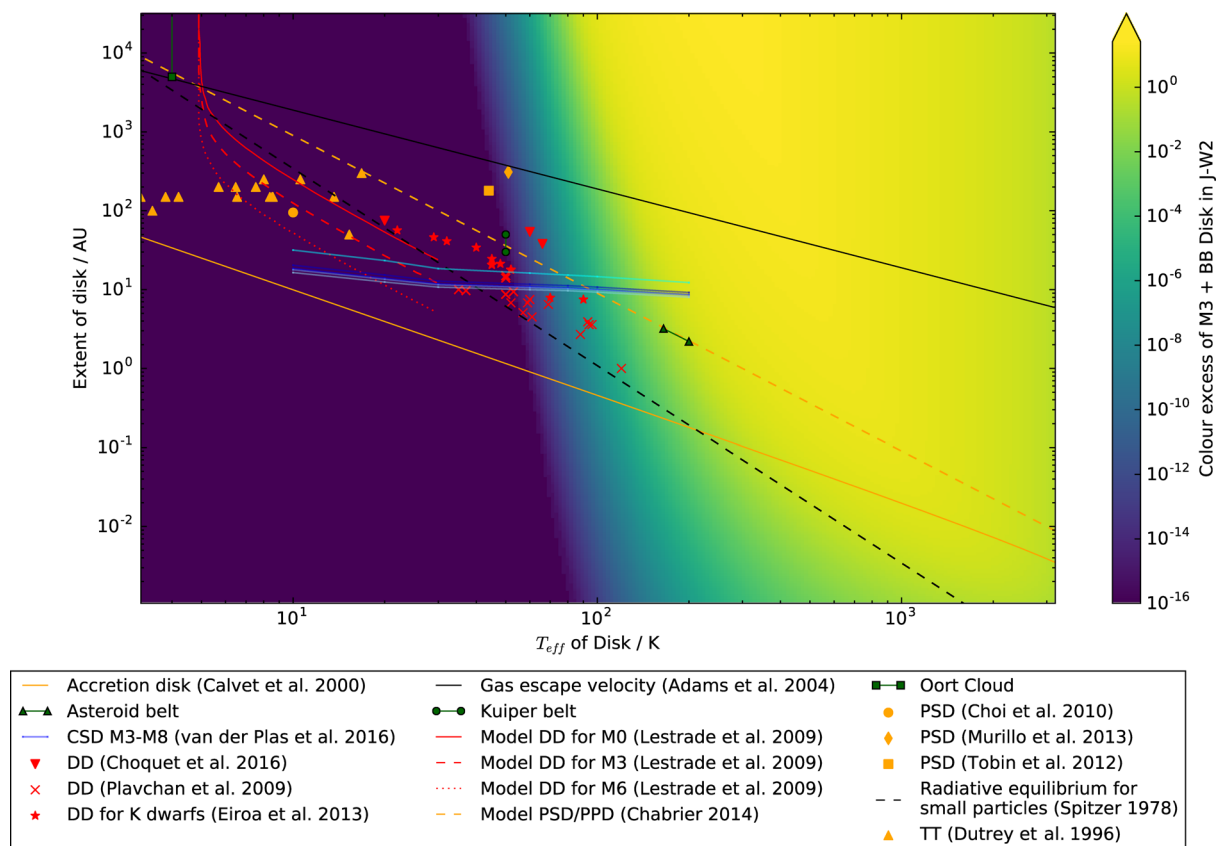
A2 Contamination from chance aligned red objects

Foreground or background objects that appear redder than our M dwarfs and are randomly aligned within the *WISE* PSF will cause
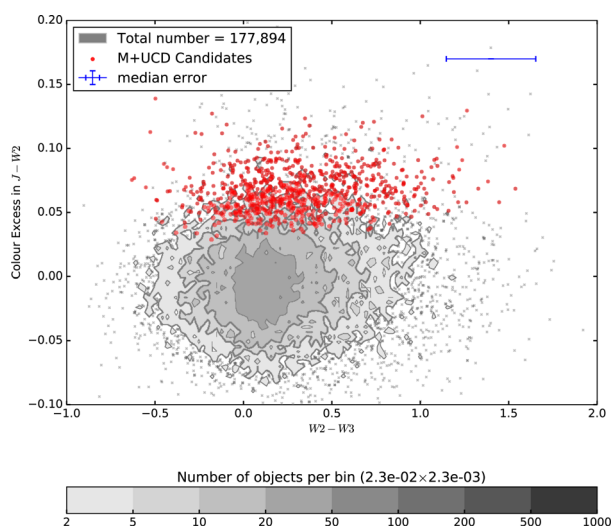
---

[4] Accessed online at https://phoenix.ens-lyon.fr/Grids/BT-Settl/

[5] 2MASS bands from http://www.ipac.caltech.edu/2mass/releases/allsky/doc/sec6_4a.html and *WISE* bands from http://wise2.ipac.caltech.edu/docs/release/allsky/expsup/sec4_4h.html

Figure A1. Simulations of the colour excess from an M dwarf with an added blackbody of temperature, T_{eff} and surface area $= \pi (\text{extent})^2$ for colour excess in $(J - W2)$. Overplotted are literature examples of circumstellar discs, CSD, debris discs, DD, protostellar discs, PSD and T-Tauri stars, TT (Dutrey et al. 1996; Plavchan et al. 2009; Choi, Tatematsu & Kang 2010; Tobin et al. 2012; Eiroa et al. 2013) and models (Spitzer 1978; Calvet et al. 2000; Adams et al. 2004; Lestrade et al. 2009; Chabrier et al. 2014; van der Plas et al. 2016). Note the Solar system objects (Asteroid belt, Kuiper belt and Oort Cloud) are plotted as comparisons to warmer stars and as such M dwarf levels of excess would be much lower.

Figure A2. Colour excess in $(J - W2)$ against $(W2 - W3)$ for all our M dwarfs in the full M dwarf candidate catalogue and for our M+UCD candidates that have a $W3$ detection. This plot shows the distribution of our M+UCD candidates is consistent with our overall distribution of M dwarfs in $(W2 - W3)$ and thus there are no obvious candidates which have extremely large $(W2 - W3)$ colour (i.e. there are no signatures of a circumstellar discs in our M+UCD candidates).

an M dwarf to look redder. We explore the various red objects, foreground and background objects that can redden our M dwarfs; we look at foreground and background M dwarf and brown dwarfs, background giants and galaxies. Although line-of-sight dust (local reddening) could also redden our M dwarfs, it is not clear how this can be easily modelled so we do not attempt this.

To calculate how many reddened objects are expected to contaminate our M dwarfs, we defined a spherical cone (Weisstein 1999) with volume, Vol. Any objects inside this spherical cone (centred around our M dwarf) appear blended due to the size of the M dwarfs PSF. This cone can also be used to calculate the density of objects in a certain area of sky, given a magnitude limit (and hence maximum distance; see equation (A3).

$$\text{Vol} = \frac{2}{3}\pi R^2 h = \frac{2}{3}\pi R^3 (1 - \cos(\theta))$$

$$\rho = \frac{N}{\text{Vol}} = \frac{N}{\left(\frac{2}{3}\pi R^3 (1 - \cos(\theta))\right)}$$

(A3)

where Vol is the volume of the spherical cone, R is the distance from the observer to the limit of visibility, N is the number of objects in the volume and θ is the angular size of the cone.

As well as being present within the PSF of *WISE*, objects need to contribute a sufficient amount of flux to give an excess in $(J - W2)$ similar to adding a UCD to our M dwarfs. We define

sufficient $(J - W2)$ excess to mean 5 per cent colour excess (see figs 6 and 7 from Paper I). Using the definition of the colour excess and adding our target M dwarf and red contaminating object in flux space leads to equation (A4), which is the limiting magnitude given a specific M dwarf and a specific $(J - W2)$ of the contaminating object that can lead to a $(J - W2)$ colour excess of, $E(J - W2)$.

$$E(J - W2) = (m_{J(M+B)} - m_{W2(M+B)}) - (m_{J(M)} - m_{W2(M)})$$

$$m_{J(M+B)} = -2.5 log_{10}(10^{-0.4 m_{J(M)}} + 10^{-0.4 m_{J(B)}})$$

$$m_{W2(B)} = -2.5 log_{10}\left(\frac{10^{-0.4(m_{J(M)} - E(J-W2))} - 10^{-0.4 m_{W2(M)}}}{1 - 10^{-0.4((J-W2)_B - E(J-W2) - (J-W2)_M)}}\right)$$
(A4)

where $m_{J(M+B)}$ and $m_{W2(M+B)}$ are the J and $W2$ magnitudes of the combined M dwarf and red contaminating object, $m_{J(M)}$ and $m_{W2(M)}$ are the J and $W2$ magnitudes of a specific M dwarf target, $(J-W2)_B$ is the colour of the red contaminating object and $m_{J(B)}$ is the limiting magnitude of the red contaminating needed to cause an Excess of $E((J-W2))$ ($\sim$0.05 for our sample).

Using equation (A4), we calculated the limiting magnitude a red contaminating object would need to have to sufficiently redden one of the M dwarfs. We chose not to apply extinction to the limiting magnitude due to the small amount of difference this would make (with an $A_V < 0.08$ and mean values of $\frac{A_\lambda}{A_V}$ of 0.179 for J and 0.056 for $W2$, see table B1 (Paper I), the extinction is of order 0.01 in J and 0.005 in $W2$).

A3 Chance alignment of brown dwarfs and M dwarfs

For chance alignments of brown dwarfs and M dwarfs, we took spatial densities from the literature (Phan-Bao et al. 2003, 2008; Cruz et al. 2007; Reid, Cruz & Allen 2007; Burningham et al. 2013, Maracco et al. 2015) and calculated the $(J - W2)$ colour of the M dwarfs and brown dwarfs from our simulated photometry (see section 3.2 Paper I); these values are presented in Table A1.

Using $(J - W2)$ from Table A1, we calculated the maximum distance brown dwarfs and M dwarfs could add sufficient flux to our target M dwarf (using equation A4). This value was used if it was brighter than the limiting magnitude in 2MASS or *WISE*; otherwise the 1.25σ 2MASS/*WISE* limit (18.05/17.00) was used instead.[6] This number was calculated for each of the 36 898 M dwarfs in our excess sample. Then using equation (A3), we estimated the number of brown dwarfs or M dwarfs chance aligned with each of our target M dwarfs. Taking the sum of the number of objects for each of our target, M dwarfs gave the total number of contaminating brown dwarfs and M dwarf expected in our M+UCD candidates. Our M+UCD candidates occupy an excess region between 0.05 and 0.15 in colour excess of $(J - W2)$. Therefore, we also subtract off those objects that have an excess greater than 0.15 to give a final number of objects. The results are shown in Table A1 and we expect a total of no more than two of our 36 898 excess sample M dwarfs to be reddened due to a chance alignment with a foreground or background M dwarf or brown dwarf.

A4 Chance alignment of M giants

For M giants we downloaded all Milky Way stars from the *10th version of the Gaia Universe Model Snapshot* (GUMS-10, Milky

Way stars in GUMS.MW; Robin et al. 2012).[7] The GUMS.MW catalogue gives simulated stellar properties such as spectral type, luminosity class and distance, as well as the predicted *Gaia G* magnitude to simulate objects present in the future *Gaia* data releases.

From this catalogue, we selected all the M giants (selecting M spectral type stars and luminosity classes I, II and III) with galactic latitude, $b > 40°$; this left 4966 M giants. We selected those with $G < 9$ (to select a complete sample at known distance) that left 3022 M giants in our M giant sample.

To work out a density, we needed a maximum distance a $G < 9$ M giant can be observed at (and thus needed the absolute magnitude of M giants in G band). Converting G in to M_G (via $M_G = G - 5 \log_{10}(\text{distance}) + 5$) and taking the faintest possible M_G value for our M giant sample (thus the worst case scenario for our density), we estimated the maximum distance *Gaia* could detect M giants to was 6983 pc. Thus the density, of M giants per parsec in a spherical cone of radius, $R = 6983$ pc, $\rho_{\text{M giant}}$ is $1.1866 \times ^{-8}$M Giants pc^{-3} (using equation A3).

To calculate the number of chance alignments of M giants with one of our M dwarfs, we needed the maximum distance we could detect M giants out to in 2MASS/*WISE*. For this, we needed the absolute magnitude of M giants. Using equation (A5) (Smart 2016)[8], we calculated an equation for J in terms of G and $(J - K_S)$ where we take the $(J - K_S)$ values for M giants from Straižys & Lazauskaitė (table 3, 2009).

$$B_J = J + 4.9816 - 0.389\,456\,70(J - K_S)$$

$$R_F = J + 2.6997 - 0.462\,578\,63(J - K_S)$$

$$M = R_F - J = 2.6997 - 0.462\,578\,63(J - K_S)$$

$$G = R_F + 0.0045 + 0.3623(B_J - R_F) - 0.1783(B_J - R_F)^2$$
$$+ 0.0080(B_J - R_F)^3$$

$$L = B_J - R_F$$

$$L = J + 4.9816 - 3.8946 \times 10^{-1}(J - K_S) - J$$
$$- 2.6997 + 4.6258 \times 10^{-1}(J - K_S)$$

$$L = 7.3122 \times 10^{-2}(J - K_S) + 2.2819$$

$$J = G - M - 0.0045 + 0.3623L - 0.1783L^2 + 0.0080L^3$$

$$J = G - 3.1278 \times 10^{-6}(J - K_S)^3 + 6.6052 \times 10^{-4}(J - K_S)^2$$
$$+ 4.8645 \times 10^{-1}(J - K_S) - 2.6976$$
(A5)

For a $(J - K_S)$ of 1.11 (average of the $(J - K_S)$ values for M giants from table 3 of Straižys & Lazauskaitė (2009) and an absolute G magnitude of -0.61, we calculate an absolute J-band magnitude of -2.7668. Feeding this in to the equation for distance $(d_J = 10^{-0.4(M_J - m_j)})$ where m_j is the 1.25σ limit of 2MASS[5] gives a distance of $\sim$200 Mpc. This distance is far beyond the reach of the Milky Way; thus, we chose to use the maximum distance observed by the excess sample, using equation (A6) taking $b_{\text{min}} = 40°$ and $h_z = 1200$ pc as stated in the GUM.MW simulation (table 2 from

---

[6] See table 1 from Paper I where we add 1.5 to convert from 5σ to 1.25σ.

[7] Accessed online at http://dc.zah.uni-heidelberg.de/__system__/dc_tables/show/tableinfo/gums.mw

[8] Equations from Smart (2016) and use transformations from http://www.astro.ku.dk/erik/Tycho-2/ and Jordi, Grebel & Ammon (2006).

Table A1. Results of the chance alignments of M dwarfs and brown dwarfs. Shown are the simulated M dwarf absolute photometry and $(J - W2)$ colour (taken from section 3.2 of Paper I), and the spatial densities taken from the literature (a. Reid et al. 2007, b. Phan-Bao et al. 2003, c. Phan-Bao et al. 2008, d. Cruz et al. 2007, e. Marocco et al. 2015, f. Burningham et al. 2013). Note space densities from Marocco et al. (2015) are stated for binary fractions of 26 ± 13 and 14 ± 10, respectively, and space densities from Burningham et al. (2013) are stated from a minimum to maximum value and we take the worst case scenario in each case to calculate the contamination. Also calculated are the limiting magnitudes to give a 5 per cent excess in $(J - W2)$ and thus the number of chance alignments of brown dwarfs and M dwarfs per target M dwarf and in total for our excess sample. Note that if the limiting magnitude was greater than the 1.25σ detection limit of 2MASS or *WISE*, the 2MASS/WISE limit (18.05/17.00) was used instead.[5]

Spectral type	M_J mag	M_{W2} mag	$(J - W2)$ mag	Spatial density $\times 10^{-3}$ pc^{-3}	$M_{J(\text{limit})}$ mag	$M_{W2(\text{limit})}$ mag	ρ^1	T[2]	Ref.
M2–M5	7.0–9.5	5.9–8.5	1.1–1.3	76	12.39–13.87	11.29–12.57	1.20×10^{-4}	1.59	a
M6–M8	10.3–11.0	9.0–9.4	1.3–1.6	4.62	13.87–16.05	12.57–14.45	4.41×10^{-6}	0.18	b
M8–L3.5	11.0–12.9	9.4–10.6	1.6–2.3	3.28	16.05–17.70	14.45–15.39	3.13×10^{-6}	0.12	c
L0–L3	11.6–12.9	9.8–10.9	1.8–2.3	1.7 ± 0.4	16.69–17.70	14.89–15.39	1.70×10^{-6}	0.05	d
L4–L6.5	13.1–14.1	10.7–11.1	2.4–3.0	0.85 ± 0.55 and 1.00 ± 0.64	17.85–18.68	15.43–15.68	6.30×10^{-7}	0.02	e
L7–T0.5	13.3–14.8	11.2–11.8	3.1–3.0	0.73 ± 0.47 and 0.85 ± 0.55	18.80–18.70	15.70–15.68	3.79×10^{-7}	0.01	e
T1–T4	14.7–14.8	11.9–12.5	2.8–2.3	0.74 ± 0.48 and 0.88 ± 0.56	18.42–17.69	15.62–15.39	1.33×10^{-7}	0.00	e
T6–T6.5	14.7–15.3	12.6–13.0	2.1–2.3	0.39 ± 0.22 to 0.71 ± 0.40	17.34–17.69	15.24–15.39	2.43×10^{-8}	0.00	f
T7–T7.5	15.6–16.0	13.1–13.3	2.5–2.7	0.56 ± 0.32 to 1.02 ± 0.64	18.01–18.29	15.51–15.59	2.51×10^{-8}	0.00	f
T8–T8.5	16.6–17.2	13.4–13.6	3.2–3.6	2.05 ± 1.21 to 3.79 ± 2.24	18.92–19.39	15.72–15.79	8.33×10^{-8}	0.00	f

[1] ρ is the number of objects per target M dwarf.
[2] Total number of objects $0.05 < E < 0.15$.

Robin et al. 2012), thus giving an observed value for the excess sample of 1 867 pc.

$$d_{\text{max}} = \frac{h_z}{\sin(b_{\text{min}})} \tag{A6}$$

The number of chance aligned giants then comes directly from equation (A3), where $\rho_{\text{M giant}}$ is $1.2 \times^{-8}$ M Giants pc^{-3}, $\theta = 6$ arcsec and $R = d_{\text{max}} = 1867$ pc. Hence, the number of chance alignments of giant stars that are sufficiently red per M dwarf is 6.8×10^{-8}. With 36 898 M dwarfs in our excess sample, we estimate $\sim$0.003 M giant chance alignments in our excess sample.

A5 Chance alignment of red galaxies

For galaxies, we started with the simulation from Henriques et al. (2012).[9] Henriques et al. (2012) use the semi-analytic models of Guo et al. (2011) that simulate the evolution of haloes and sub-haloes within them. These models are implemented on two large dark matter simulations, the Millennium Simulation (Springel et al. 2005) and Millennium-Iwe Simulation (Boylan-Kolchin et al. 2009).

This gave us access to distance, J_{AB}, the Spizter [4.5μm] band (also in the AB system, and assumed for simplicity to have a similar band-pass to $W2$). We chose to only count galaxies initially brighter than the *WISE* $W2$ 1.25σ limit (see table 1 from Paper I where we add 1.5 to convert from 5σ to 1.25σ) of 17 and a $(J - W2)$ colour redder than 1.17 (the bluest colour our M+UCD candidates appear to be).

$$J_{AB} = J_{\text{Vega}} + 0.91$$

$$W2_{AB} = W2_{\text{Vega}} + 3.339$$

$$(J - W2)_{AB} = (J - W2)_{\text{Vega}} - 2.429$$

$$[4.5\,\mu\text{m}] < 20.4 \qquad J - [4.5\,\mu\text{m}] > -1.259 \tag{A7}$$

These needed to be converted into the AB system; for $W2$ this was done using equation (A7) (from Jarrett et al. 2011)[10] and for J this was done using equation (A7) (from Blanton & Roweis 2007).[11] This led to a $(J - W2)$ conversion shown in equation (A7), and the cuts were then applied to the simulations by Henriques et al. (2012). This left 11 903 galaxies in our sample of red galaxies.

Galaxies can be red for a number of reasons (i.e. galaxies can be red because they are dusty, which reddens starlight and also emits in the infrared and via reddening due to redshift); to keep the estimation of contamination as simple as possible, we use our sample of red galaxies to model the spread in $(J - W2)$ observed. We took the minimum, mean and maximum values of the $(J - W2)$ galaxy distribution and calculated the limiting magnitude in J band (using equation A4) that would give an excess of 5 per cent. This value was used as a new cut to the galaxy sample if the galaxy was brighter than the 1.25σ limiting magnitude in 2MASS[5]; otherwise the 1.25σ 2MASS/WISE band limit (18.05/17.00) was used. The number of objects left gave the density of objects out to the limiting magnitude in which the galaxies would redden our M dwarfs by 5 per cent (see Table A2).

There were two ways to convert this number into a number of objects chance aligned with one of our M dwarfs. Taking all galaxies to be at infinite distance, one can simply divide the area of the *WISE* PSF (6 arcsec) by the area of the survey (1°.4 × 1°.4); however, for consistency we also work out a density of galaxies and use the spherical cone analysis. Using the sample of galaxies we calculated the minimum, mean and maximum absolute J-band magnitudes and thus the minimum, mean and maximum values for the distance of these galaxies. Then using equation (A3), we estimated a density, and the number of galaxies per M dwarf, and in the total excess sample (of 36 898 M dwarfs). All results for the minimum, mean and maximum values can be seen in Table A2.

In our selection process (Paper I), any galaxy that looked extended in 2MASS or *WISE* was rejected as a contaminant and thus

Table A2. Table showing the limiting magnitudes to give a five per cent excess in $(J - W2)$ and thus the number of chance alignments of galaxies per target M dwarf and in total for our excess sample. Note that if the limiting magnitude was greater than the 1.25σ detection limit of 2MASS or *WISE*, the 2MASS/*WISE* limit (18.05/17.00) was used instead.[5]

	Unit	Minimum	Mean	Maximum
$(J - W2)$	mag	1.43	2.65	3.93
$M_{J(\text{limit})}$	mag	15.15	18.22	19.76
$M_{W2(\text{limit})}$	mag	13.72	15.57	15.83
1.25σ 2MASS limit	mag	18.05	18.05	18.05
1.25σ *WISE* limit	mag	17	17	17
Number of red galaxies in survey		39	898	1207
Density of red galaxies	Mpc^{-3}	0.001	0.015	0.020
Number of objects per target M dwarf		1.74×10^{-4}	4.00×10^{-3}	5.37×10^{-3}
Total objects in with $E > 0.05$		10	143	175
Number of extended ($\theta > 3$ arcsec)		10	21	21
Total objects with $E > 0.15$		0	28	42
Total non-extended objects $0.05 < E < 0.15$		0	94	112

rejected from our excess sample. We thus also need to remove any galaxies in our sample that appear extended in 2MASS or *WISE* and thus already rejected from amongst our M dwarfs. To do this, we use the hydrodynamic cosmological simulation from fig. 3 of Naab, Johansson & Ostriker (2009) to define a relationship between redshift, z and extent of the galaxy (see equation A8).

$$\left[\frac{\text{extent}}{\text{kpc}}\right] = -1.1551\log_{10}(z) + 1.2985 \quad \text{correlation} = -0.97$$

$$(A8)$$

However, one must be careful in converting extent of a galaxy as the angular size varies as a function of redshift (see equation A9 from equations 7.33, 7.37, 7.31 and 7.11; Ryden & Partridge 2004),

$$\theta = \left[\frac{\text{extent}}{d_A}\right]^{\text{rad}}$$

$$d_A = \frac{d_L}{(1+z)^2}$$

$$d_L \approx \frac{c}{H_0}z\left(1 + \frac{1+q_0}{2}z\right)$$

$$q_0 = \Omega_{r,0} + 0.5\Omega_{m,0} - \Omega_{\Lambda,0} \quad (A9)$$

where d_A is the angular diameter distance, d_L is the luminosity distance, z is the redshift, θ is in radians, $H_0 = 72$ km s^{-1} Mpc^{-1}, $q_0 = -0.55$ is the deceleration parameter for $\Omega_{\Lambda,0} = 0.7$, $\Omega_{m,0} = 0.3$ and $\Omega_{r,0} = 0$ for a nearly flat universe. Combining the equations in equation (A9) gives an equation for $\theta = \theta(z)$. Taking the PSF of 2MASS as 3 arcsec, this is equivalent to galaxies of redshift smaller than 0.05 as being possibly extended and thus already rejected.

Our M+UCD candidates occupy an excess region between 0.05 and 0.15 in colour excess of $(J - W2)$. Therefore, we also subtract off those objects that have an excess greater than 0.15 to give a final number of objects. Hence, the number of chance alignments is 4×10^{-3} per M dwarf. With 36 898 M dwarfs in our excess sample, we estimate a worst case scenario of between 94 and 112 of our excess sample may be reddened by chance alignments with red galaxies.

A6　Chance alignment from random offsets

Another way we gauge possible contamination from red objects was to randomly offset our excess sample by $2°$ at random angles. This movement to a random location should simulate the possibility of finding a chance aligned object. We then cross-matched these offset

points with *WISE* (out to six arcsec totalling 3073 of 36 898 matches) and with 2MASS (out to 3 arcsec totalling 464 of the 3073 matches). We were then able to work out $(J - W2)$ colour of these objects. From this, we added the object back to our M dwarfs $(J - W2)$ and thus were able to calculate the objects colour excess. Of the 464 objects that had a random object with both a *WISE* and 2MASS detection, 105 had a positive non-zero excess and 38 had an excess between 0.05 and 0.15 (equivalent to our improvement contour constraints). Thus, a total of 0.285 per cent and 0.103 per cent of our M dwarf in our excess sample had chance alignments (out of the total 36 898). This means out of our 1082 M+UCD candidates we would have 105 objects (9.70 per cent) due to chance alignments that would produce a positive non-zero excess and 38 objects (3.51 per cent) that would produce an excess that matched our contour criteria and be selected by our approach. Thus, we can expect a contamination from chance alignments of around 3.5 per cent and no worse than $\sim$9.5 per cent.

A7　Visual inspection of the M+UCD candidates

As part of our reduction in contamination, we visually inspected[12] our M+UCD candidates in SDSS (g, r), in 2MASS (J, H), in *WISE* ($W1$, $W2$ and $W3$) and where possible in UKIDSS J (Lawrence et al. 2007, 2013) and the DSS2 red band. We flagged any object that was obviously blended by a red galaxy, by a diffraction spike from a bright nearby star, both of which are obvious contamination. We also flagged any object blended by a nearby object; these are also probably contamination but are not removed from our catalogue completely (due to the unknown contribution such an object gives to our M dwarf). Of our 1 082 M+UCD candidates, we found:

(i) 161 (14.88 per cent) as having nearby sources within the size of the *WISE* PSF and being possible blends;

(ii) 29 (2.68 per cent) as having identifiable nearby galaxies as possible blends;

(iii) 3 (0.28 per cent) as having possible contamination from the diffraction spikes of nearby bright stars;

(iv) 11 (1.02 per cent) as having other problems (i.e. no images or too faint to identify in one or more of the images).

---

[12] This was achieved by using the PYTHON module ASTROQUERY SKYVIEW http://dx.doi.org/10.6084/m9.figshare.805208

These numbers seem high; however, although any of these blended sources may contribute to the reddening of our M dwarfs, they also might not (since the effects of the blend on the data quality are not known directly) and thus we use this number as a rough estimate of possible blended contamination. The visual inspection of the UKIDSS images (143 of the 1082 had UKIDSS images) also showed 27 close blends; 25 of these nearby objects have the UKIDSS photometry (obtained by cross-matching with *UKIDSS Large Area Survey*, UKIDSS LAS; Lawrence et al. 2007, 2013). We then located any UKIDSS source that was within the *WISE* PSF and found 31 other sources around our 25 objects with the UKIDSS photometry. 19 of these were flagged as galaxies using the PGALAXY[13] flag greater than 0.5; however, as some of these nearby sources are blended with our M dwarfs, they may be misclassified as galaxies.

To gauge an upper limit on how many galaxies might be in our M+UCD candidates, we cross-matched our M+UCD candidates with UKIDSS LAS (again within the *WISE* 6 arcsec PSF); 247 had matches with our 1082 M+UCD candidates. Around these 247 M dwarfs were 175 sources detected within the *WISE* PSF, of which 85 were flagged as galaxies (PGALAXY>0.5). Thus, an upper limit on the number of galaxies would be 372 (34.4 per cent); however, as we discussed in Section A5, one needs to take into account that many of these galaxies will not have the correct $(J − W2)$ to give a colour excess that could mimic an unresolved UCD companion.

---

[13] PGALAXY is calculated by combining individual detection classifications in the source merging process see http://wsa.roe.ac.uk/www/gloss_p.html#lassource_pgalaxy for the definition.

This paper has been typeset from a TEX/LATEX file prepared by the author.